The *Arabidopsis* D-Type Cyclin CYCD2;1 and the Inhibitor ICK2/KRP2 Modulate Auxin-Induced Lateral Root Formation [C][W][OA]

Luis Sanz,[a,b,1] Walter Dewitte,[a,1] Celine Forzani,[a] Farah Patell,[a] Jeroen Nieuwland,[a] Bo Wen,[a] Pedro Quelhas,[c] Sarah De Jager,[d] Craig Titmus,[a] Aurélio Campilho,[c,e] Hong Ren,[f] Mark Estelle,[f] Hong Wang,[g] and James A.H. Murray[a,2]

[a] Cardiff School of Biosciences, Cardiff University, CF10 3AX Cardiff, United Kingdom
[b] Centro Hispano Luso de Investigaciones Agrarias, Universidad de Salamanca, 37185 Salamanca, Spain
[c] Instituto de Engenharia Biomédica, Divisão de Sinal e Imagem, 4200-465 Porto, Portugal
[d] Department of Physiology, Development, and Neuroscience, University of Cambridge, CB2 3DY Cambridge, United Kingdom
[e] Universidade do Porto, Faculdade de Engenharia, 4200-465 Porto, Portugal
[f] Division of Biological Sciences, University of California–San Diego, La Jolla, California 92093-0116
[g] Department of Biochemistry, University of Saskatchewan, Saskatoon, Saskatchewan S7N 5E5, Canada

The integration of cell division in root growth and development requires mediation of developmental and physiological signals through regulation of cyclin-dependent kinase activity. Cells within the pericycle form de novo lateral root meristems, and D-type cyclins (CYCD), as regulators of the G_1-to-S phase cell cycle transition, are anticipated to play a role. Here, we show that the D-type cyclin protein CYCD2;1 is nuclear in *Arabidopsis thaliana* root cells, with the highest concentration in apical and lateral meristems. Loss of CYCD2;1 has a marginal effect on unstimulated lateral root density, but CYCD2;1 is rate-limiting for the response to low levels of exogenous auxin. However, while *CYCD2;1* expression requires sucrose, it does not respond to auxin. The protein Inhibitor-Interactor of CDK/Kip Related Protein2 (ICK2/KRP2), which interacts with CYCD2;1, inhibits lateral root formation, and *ick2/krp2* mutants show increased lateral root density. ICK2/KRP2 can modulate the nuclear levels of CYCD2;1, and since auxin reduces ICK2/KRP2 protein levels, it affects both activity and cellular distribution of CYCD2;1. Hence, as ICK2/KRP2 levels decrease, the increase in lateral root density depends on CYCD2;1, irrespective of ICK2/CYCD2;1 nuclear localization. We propose that ICK2/KRP2 restrains root ramification by maintaining CYCD2;1 inactive and that this modulates pericycle responses to auxin fluctuations.

INTRODUCTION

Roots grow due to cell division in the meristem located at the root tip and the subsequent expansion of these cells immediately behind this division zone. The ramification of the root system due to the formation of lateral roots is essential to form a dense network allowing for effective anchorage and exploration of the soil for uptake of water and minerals and is consequently very important for the survival of the plant. The initiation of lateral roots occurs from nondividing cells distal to the root meristem, and the modulation of this process allows adaptation of the root system to the heterogeneous and changing environment of the soil. Lateral root development is therefore influenced by a range of factors, including nutrient and water availability and the physical

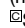structure of the substrate (López-Bucio et al., 2003; Péret et al., 2009).

Lateral roots are initiated from specific cells within the pericycle, a cell layer surrounding the central stele of the root. The pericycle cells lying on the xylem axis and, hence, adjacent to the xylem poles specifically participate in the process of lateral root initiation. These cells maintain the potential to reactivate cell division and initiate a new root meristem de novo, and it has been proposed that separable priming of founder cells first establishes a pattern of primed cells within a region known as the basal meristem (De Smet et al., 2007) or transition zone (Baluska et al., 2010), where cell division is slowing.
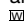
These primed cells then reinitiate division as they are displaced further up the root into the lateral root initiation zone (Casimiro et al., 2003). This unique process of lateral root initiation in the pericycle, whereby cells are first specified and then subsequently resume division and acquire new fates, is thus an interesting model for cellular responses to mitogenic signals (Péret et al., 2009). Different models of the underlying mechanism for spatio-temporal distribution of lateral roots have been postulated. Auxin signaling linked with oscillations in auxin levels has been considered the major factor in the priming of lateral root founder cells (De Smet et al., 2007; Dubrovsky et al., 2008; Fukaki and Tasaka, 2009; Péret et al., 2009), but recently it has been proposed that
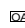
oscillating gene expression determines spacing of future lateral roots by specifying prebranch sites, and this oscillation appears to be governed by an endogenous mechanism. Auxin at concentrations within the physiological range is not sufficient to specify prebranch sites, but auxin is able to modulate the location of prebranch sites (Moreno-Risueno et al., 2010).

Mutants in the auxin perception or response pathways are often affected in lateral root formation, and mutants in *AUX/IAA14* (*SOLITARY ROOT*) lack lateral roots. Conversely, treatment of roots with high levels of auxin triggers ectopic lateral root initiation and activation of all pericycle cells (Himanen et al., 2002), a phenotype also seen in the auxin overproducing *superroot* mutant (Boerjan et al., 1995). At lower auxin levels, lateral root primordia form on sites marked by local auxin response maxima induced by bending (Ditengou et al., 2008; Laskowski et al., 2008). Furthermore, regulation of lateral organogenesis by auxin involves several successive response pathways (De Smet et al., 2010).

The onset of lateral root primordium formation starts with the occurrence of a series of anticlinal, asymmetric divisions in the pericycle cell file adjacent to the xylem poles in response to auxin (Laskowski et al., 1995; Dubrovsky et al., 2001). Treating roots with auxin induces divisions in the pericycle outside the root apical meristem (RAM), and the pericycle cells at the xylem poles are particularly responsive (Laskowski et al., 1995). However, although cell division is required for the formation of multicellular primordia, triggering the cell cycle in the pericycle cells is not sufficient by itself to induce primordium initiation (Vanneste et al., 2005). Nevertheless, it is clear that the formation of primordia is closely linked to induction of the cell cycle.

Progression through the major phases of the cell cycle (G_1, S, G_2, and M) is regulated by cyclin-dependent kinase complexes, composed of catalytic cyclin-dependent kinase (CDK) and regulatory cyclin subunits. Commitment of cells to the cell cycle and progression to the G1-to-S phase transition is regulated primarily by CDKA through its association with D-type cyclins (CYCDs). The primary phosphorylation target of CDKA-CYCD is the RETINOBLASTOMA-RELATED (RBR) protein, itself a repressor of the cell cycle–promoting action of E2F/DP transcription factors. Modulation of CDK activity is not only achieved by modulating the levels of the CDK and cyclin subunits, but also by intracellular localization, posttranslational modification such as phosphorylation, and interactions with proteins of the Interactor of CDK/Kip-Related Protein (ICK/KRP) and SIAMESE families (Dewitte and Murray, 2003; Churchman et al., 2006; Inzé and De Veylder, 2006). High levels of ICK/KRP proteins inhibit the G1-to-S phase transition of both the mitotic cell cycle and the endocycle, a shunted cell cycle in which mitosis is omitted, whereas a moderate increase affects mainly mitotic cell cycles (Verkest et al., 2005b). The levels of ICK1/KRP1 and ICK2/KRP2 proteins are posttranslationally regulated by proteolysis (Verkest et al., 2005b; Jakoby et al., 2006), and ICK2/KRP2 proteolysis is dependent on CDK-mediated phosphorylation (Verkest et al., 2005b). Both ICK1/KRP1 and ICK2/KRP2 interact with CDKA and CYCD (Zhou et al., 2002), and both ICK/KRP proteins are nuclear localized (Bird et al., 2007). ICK1/KRP1 requires nuclear localization to be active and is subjected to proteasomal degradation in the nucleoplasm (Jakoby et al., 2006). ICK1/KRP1 has been shown to interact with CDKA in the cyto-plasm and mediate nuclear transport of CDKA (Jakoby et al., 2006; Zhou et al., 2006).

Auxin treatment of roots induces rapid changes in several core cell cycle regulators (Himanen et al., 2002). This work showed that auxin-induced lateral root formative divisions in the pericycle are associated with downregulation of transcripts encoding several of the ICK/KRP proteins. However, the molecular mechanisms at the interface of the cell cycle machinery leading to cell cycle activation for lateral root formation, the priming of lateral root founder cells, and the basis of auxin response sensitivity in the pericycle are still largely unknown. There is a functional linkage between these processes, since increasing levels of the G1-S phase regulators CYCD3;1 or E2F/DP by ectopic overexpression, while in itself not sufficient to induce lateral roots, enhances the response of pericycle cells to auxin (De Smet et al., 2010).

CYCDs interact with ICK/KRP proteins (Zhou et al., 2002), and increased CYCD levels can suppress the negative effects of elevated ICK/KRP levels on plant growth (Jasinski et al., 2002; Zhou et al., 2003). Through their association with CDKA, CYCDs control entry into the mitotic cell cycle and the transition of cells through G1-phase into S-phase (Riou-Khamlichi et al., 1999, 2000; Dewitte et al., 2003, 2007; Masubelele et al., 2005; Menges et al., 2006) and are therefore key candidates for regulating pericycle cell responses. The *Arabidopsis thaliana* genome encodes 10 genes for D-type cyclins, and extensive research mainly in cell cultures has revealed regulation by external signals and a degree of dependence on cell cycle phase (Riou-Khamlichi et al., 1999, 2000; Healy et al., 2001; Menges et al., 2005). Of these, only *CYCD4;1* is known to have a role in root architecture, being required for the increase in lateral root density in response to Suc (Nieuwland et al., 2009). *CYCD4;1* is induced by Suc, and *cycd4;1* mutants or wild-type roots grown on low Suc have reduced lateral root density, associated with an earlier transition of the pericycle cell file from the apical to the basal meristem in which cell expansion initiates. Since the basal meristem cells are also larger, this leads to reduced cell density in this region and fewer lateral root priming events (Nieuwland et al., 2009). However, *CYCD4;1* is not required for the increasing lateral root density in response to applied auxin, and the mutant phenotype is rescued by application of low levels of exogenous auxin [10 nM 2-(1-naphthyl)acetic acid (NAA)].

CYCD2;1 is an interesting candidate to be involved in cell cycle stimulation in the various root tissues. Like the related *CYCD4;1* gene, transcription of *CYCD2;1* is upregulated by Suc but not by hormones (Riou-Khamlichi et al., 2000; Nieuwland et al., 2009). Elevating CYCD2;1 levels triggers divisions in the RAM (Qi and John, 2007), and expression of *Arabidopsis* CYCD2 shortens the G1-phase in tobacco (*Nicotiana tabacum*) roots (Cockcroft et al., 2000). CYCD2;1/CDKA activity is able to phosphorylate RBR, which is involved in G1-phase cell cycle arrest and can be inactivated by hyperphosphorylation (Hirano et al., 2008). Furthermore, CYCD2;1/CDKA complexes are able to sequester ectopically expressed ICK1/KRP1 protein (Ren et al., 2008), which inhibits lateral root formation when overexpressed. Unlike other D-type cyclins, such as CYCD3;1, it appears to be a relatively stable protein (Healy et al., 2001; Planchais et al., 2004).

Here, we show that CYCD2;1 and ICK2/KRP2 are genetically interacting components involved in lateral root induction in response to auxin. We propose a model in which the auxin-mediated

regulation of *ICK2/KRP2* contributes to lateral root density increases, dependent on CYCD2;1 levels.

RESULTS

CYCD2;1 Accumulates in Root Meristem Cell Nuclei

To reveal the localization of CYCD2;1, we expressed a fusion of the full-length genomic sequence of *Arabidopsis CYCD2;1* to green fluorescent protein (GFP) under the control of the native *CYCD2;1* promoter and 5′ untranslated region consisting of 3970 bp upstream of the start codon (*ProCYCD2;1:CYCD2;1-GFP*). Expression of *CYCD2;1* cDNA in *Arabidopsis* results in truncated transcripts due to alternative splicing (Qi and John, 2007), but the expression of the genomic version fused to enhanced *GFP* under control of its native promoter and untranslated region resulted in the presence of normally spliced mRNAs with transcripts of the expected length (Figure 1C) and the accumulation of full-length CYCD2;1 protein fused to GFP with a size of 75 kD (Figure 1D). We also noted the presence of a shorter protein recognized by the anti-CYCD2;1 antiserum (Figure 1D), but as it was not recognized by the anti-GFP antibody (Figure 6C), it is unlikely to contribute to GFP fluorescence. Quantitative RT-PCR measurements revealed a five- to sixfold overall increase of total *CYCD2;1* transcripts in the *ProCYCD2;1:CYCD2;1-GFP* line used for further experimentation compared with nontransformed controls (Figure 1E), indicating a mild level of overexpression.

In roots of seedlings 5 d after germination (DAG), we observed accumulation of CYCD2;1 protein in all cell files of the root apical and basal meristems (Figure 1A). In most tissues of the meristem, apart from the quiescent center, adjacent initials and their immediate progeny, where the signal was weaker and/or more diffuse, CYCD2;1 appeared to be predominantly nuclear (Figure 1G). The same observations were made in 25 independent T1 transformants. Further up the meristem, where cells of the cortex and epidermis elongate, the nuclear CYCD2;1-GFP signal became gradually weaker, and the level dropped in cortical cells concomitant with the increase in cell elongation (Figure 1B). We noted that fluorescence of nuclear CYCD2;1-GFP declined more slowly in the endodermis compared with other tissues (Figure 1A, arrows) and was detectable outside the meristem in all root tissues, albeit it at a lower level.

Outside the root meristem, CYCD2;1 expression was maintained in the mature pericycle cells, in cells forming lateral root primordia and in adjacent vascular tissues (Figures 1I to 1L). We observed that nuclei of pericycle cells that are primed for asymmetric division in the basal meristem (De Smet et al., 2007) were marked by nuclear CYCD2;1-GFP (Figure 1I), as were the nuclei in phase II primordia (Péret et al., 2009) and in the surrounding vascular tissues (Figures 1J and 1K). Upon penetration of the epidermis by the emerging lateral root phase VIII primordium, the lateral root tip was marked by nuclear CYCD2;1-GFP, again with a lower level in the columella, as observed in the primary root meristem (Figure 1L, arrow).

In mature root tissues, the highest level of CYCD2;1-GFP was observed in the endodermis (Figure 1H, arrows), but CYCD2;1-GFP was also detected in the pericycle. These observations indicate that in the postembryonic root, CYCD2;1 accumulates in the nucleus in most tissues and that the highest levels of CYCD2;1 are found in cells of the apical and lateral root meristems.

Intracellular Distribution of CYCD2;1 Is Cell Cycle Phase Dependent

In the proximal meristem close to the quiescent center, CYCD2;1 was nuclear in most cells. However, in a few meristem cells, CYCD2;1-GFP was cytoplasmic (Figure 1G, inset). This localized or spotty absence of nuclear signal was apparent in all cell files and suggests that CYCD2;1 nuclear localization could be linked to cell cycle position. To monitor cell cycle progression, we introduced the chromatin marker *35S:H2B-YFP* (for yellow fluorescent protein) (Boisnard-Lorig et al., 2001) into the *ProCYCD2;1:CYCD2;1-GFP* line (Figure 1F). Examination of the cortex and endodermal cell files, in which the majority of cells are in G_1 (Willemse et al., 2008) in the proximal meristem, showed that CYCD2;1 was exclusively nuclear in G_1 and disappeared from the nucleus after DNA replication and before chromosome condensation during prophase, as determined from the elevated signal of the H2B-YFP marker corresponding to a G_2 DNA content. When cells again reached the G_1-phase, CYCD2;1-GFP reaccumulated in the nucleus (Figure 1F). These observations suggest that CYCD2;1 has a dynamic localization during cell cycle progression and is nuclear in G_1, and loses its chromatin association shortly before or during M-phase.

CYCD2;1 Accumulation Requires Suc

Carbon source availability in the form of Suc is likely to be a major determinant of cell division and regulates expression of the *Arabidopsis* D-type cyclins *CYCD2;1*, *CYCD3;1* (Riou-Khamlichi et al., 2000), and *CYCD4;1* (De Veylder et al., 1999; Nieuwland et al., 2009). To understand the regulation of CYCD2;1 protein level in response to Suc, we examined the effect of Suc removal on the abundance of CYCD2;1 protein (Figure 2A). *ProCYCD2;1: CYCD2;1-GFP* plants were germinated and grown in total darkness for 5 d on medium lacking Suc to avoid sugar biosynthesis driven by photosynthesis and to deplete plants of carbohydrate reserves. The levels of CYCD2;1-GFP in these dark-grown plants were drastically reduced (Figure 2A, top right panel). Within 6 and 12 h of transfer to a medium containing Suc, CYCD2;1-GFP was induced, as GFP fluorescence accumulated in the nuclei of the root meristem cells (Figure 2A, right panels). No induction could be detected in roots of seedlings transferred to medium lacking Suc (Figure 2A, bottom left panels). We conclude that CYCD2;1 protein levels depend on sugar availability, and since *CYCD2;1* mRNA levels respond in seedlings to Suc (Riou-Khamlichi et al., 2000), this suggests a close correlation between transcriptional activation by sugars (Riou-Khamlichi et al., 2000) and the accumulation of CYCD2;1 protein in these root tissues.

CYCD2;1 Degradation Depends on Activity of the 26S Proteasome

To investigate whether the CYCD2;1 turnover is dependent on proteasome activity, we treated plants with MG132, an inhibitor of proteasome activity. Five DAG *ProCYCD2;1:CYCD2;1-GFP* seedlings were transferred to fresh medium in the presence or
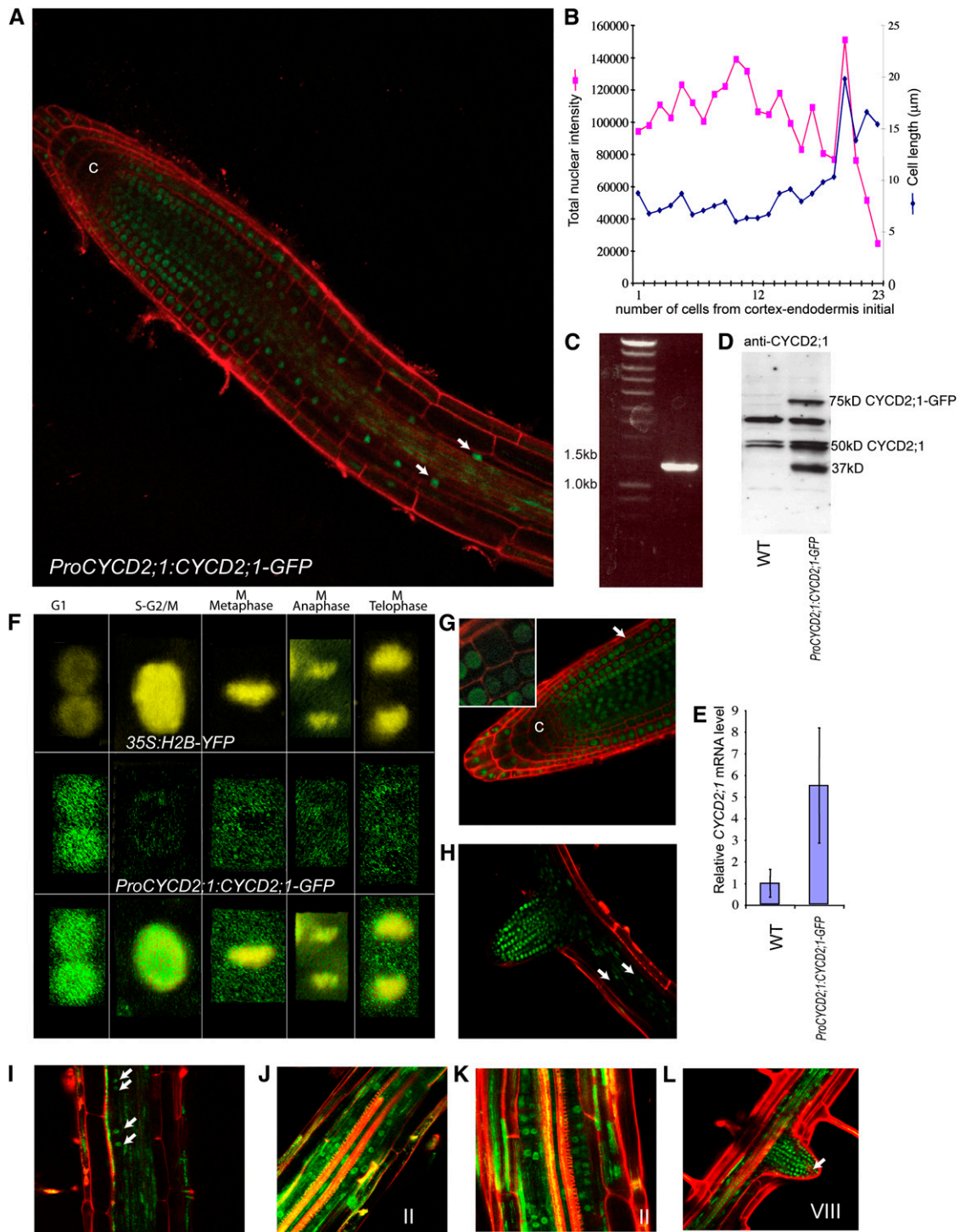
Figure 1. CYCD2;1 Distribution in *Arabidopsis* Roots.

(A) and **(B)** *ProCYCD2;1:CYCD;1-GFP* expression results in nuclear accumulation of CYCD2;1-GFP in cells of the apical and lateral meristems apart from the columella (c). Signal is also detectable at lower levels in elongated tissues, where the strongest fluorescence is found in the endodermis (**[A]** and **[H]**, arrows). For all tissues, the CYCD2;1-GFP signal declines upon exit from the apical meristem, as illustrated by associating the total nuclear fluorescence intensity for cells of the cortex from the cortical-endodermal initial cell (cell 1) to cell 23 to the cell length **(B)**.

(C) to **(E)** *ProCYCD2;1:CYCD2;1-GFP* expression results in increased levels of full-length *CYCD2;1* transcripts and protein.

(C) RT-PCR reaction using a 5′ forward primer recognizing the start of the *CYCD2;1* coding sequence and a 3′ reverse GFP primer results in a product

absence of MG132. After 12 h, there was an increase in detectable CYCD2;1-GFP protein in RAM and vascular tissues in comparison to untreated control roots (Figure 2B). Using immunoblot analysis with anti-CYCD2;1 antiserum, we could detect accumulation of CYCD2;1 in wild-type seedlings after inhibiting the 26S proteasome with MG132 (Figure 2C). In a separate experiment, we examined CYCD2;1 levels in the *axr1-3* mutant, which is impaired in the RUB conjugation pathway required for normal E3 ubiquitin protein ligase function (Petroski and Deshaies, 2005; Dharmasiri et al., 2007). An increase in CYCD2;1 was observed (Figure 2D), consistent with the conclusion that CYCD2;1 is degraded by a proteasome-dependent mechanism, as previously concluded for CYCD3;1 (Lechner et al., 2002; Planchais et al., 2004).

CYCD2;1 Is Rate-Limiting for Auxin-Induced Lateral Root Formation

Enhanced CYCD2;1 levels trigger additional cell divisions in the RAM without affecting the overall root growth rate (Qi and John, 2007). To analyze CYCD2;1 roles further, we identified a *cycd2;1* mutant allele with loss of *CYCD2;1* function (see Supplemental Figures 1B and 1E online). No obviously apparent growth or development phenotype was observed, and no clear differences in longitudinal growth of the primary root between the *cycd2;1* mutant and the wild type were detected under standard experimental conditions (Figure 3A), nor could we detect a significant difference in the number of mitotic events in the RAM, since in *cycd2;1* roots an average of 10.5 (SE = 1.4) mitotic events/root tip was observed compared with 10.8 events/tip in the wild type (SE = 1.8; P = 0.9). However, in the *ProCYCD2;1:CYCD2;1-GFP* line, which has a fivefold increase of *CYCD2;1* transcripts as discussed above, the number of mitotic figures in root tip squashes increased from 10.8 (wild type) to 14.5 (SE = 1.0; P = 0.1) in the fusion line. This was associated with a threefold increase in the level of transcripts of the G2/M marker *CYCLINB1;1* in *ProCYCD2;1:CYCD2;1-GFP* root extracts, leading us to conclude that CYCD2;1 is not required for the normal rate of cell division in the RAM, but an increase is able stimulate additional divisions in the RAM, consistent with results from constitutive overexpression of *CYCD2;1* with the 35S promoter (Qi and John, 2007).

Since lateral roots are initiated by anticlinal and periclinal cell divisions in the pericycle (De Smet et al., 2006) and this initiation is dependent on and stimulated by auxin (Casimiro et al., 2001), we tested whether or not the *cycd2;1* mutant responds differently to auxin treatment in terms of lateral root initiation. Under standard conditions, lateral root density after 10 d was marginally lower (10% decrease, P = 0.01) in the *cycd2;1* mutant line and unchanged in the *ProCYCD2;1:CYCD2;1-GFP* line compared with the density of emerged lateral roots in the wild type (Figure 3B). However, lateral root development in the gain- and loss-of-function mutants of *CYCD2;1* responded differently to auxin (Figure 3D). The differences in lateral root density between the wild type and *cycd2;1* or between *ProCYCD2;1:CYCD2;1-GFP* and the wild type increased, both in relative and in absolute terms, and became highly significant when grown on 10 to 100 nm NAA (P < 0.0001; Figure 3D). Growing the wild type on media with 100 nM auxin increased the lateral root density eightfold (mean 8.04 lateral roots/cm) after 8 d, compared with sixfold in the *cycd2;1* mutant (mean 6.53 lateral roots/cm, 19% decrease), whereas the primary root growth was the same in both backgrounds (Figure 3C). Interestingly, introducing the *CYCD2;1-GFP* fusion under control of its native promoter in the wild type, which results in a five- to sixfold increase of *CYCD2;1* transcripts (Figure 1E), conferred an increased auxin response in terms of lateral root development (mean *ProCYCD2;1:CYCD2;1-GFP* = 9.59 lateral roots/cm, 19% increase; Figure 3D).

Our analysis did not show an upregulation of *CYCD2;1* protein or transcript levels after 24 h of auxin stimulation (see Supplemental Figures 1A and B online). However, in line with previous reports (Himanen et al., 2002), treatment with 100 nM NAA induced *CYCB1;1* (see Supplemental Figure 1A online) in these experiments, indicating that cell cycle activity is indeed upregulated upon transfer to auxin. In conclusion, although *CYCD2;1* expression is not directly regulated by auxin, *CYCD2;1* contributes to the sensitivity of the pericycle cell response to auxin.

CYCD2;1 Is Able to Interact with KRP Proteins

CDK inhibitory proteins, such as ICK/KRPs, have been proven to be potent inhibitors of the cell cycle in *Arabidopsis* at elevated

---

Figure 1. (continued).

(right lane) with expected size for full-length *CYCD2;1* transcripts of 1346 nucleotides, with no evidence of the aberrant splicing that would result in a truncated protein as reported for expression of the *CYCD2;1* cDNA (Qi and John, 2007). The molecular mass marker is shown in the left lane.

(D) Protein gel blot analysis using anti-CYCD2;1 antiserum of extracts from the untransformed wild type (WT; left lane) and *ProCYCD2;1:CYCD2;1-GFP* line (right lane) confirms the presence of a predicted full-length 75-kD CYCD2;1-GFP fusion protein.

(E) Quantitative PCR quantification of total *CYCD2;1* transcripts reveals a five- to sixfold upregulation in the *ProCYCD2;1:CYCD2;1-GFP* line compared with the wild type; error bars represent SE on three biological replicates.

(F) and **(G)** The intracellular distribution of CYCD2;1-GFP is cell cycle phase dependent. CYCD2;1-GFP leaves the nucleus prior to or during early prophase and reenters the nucleus during G_1 **(F)**, which results in the occasional absence of nuclear CYCD2;1-GFP in meristem cells **(G)** and inset detail. Top row of **(F)**, H2B-YFP reveals the chromatin; middle row of **(F)**, localization of CYCD2;1-GFP during the cell cycle; and bottom row of **(F)**, merged signals.

(H) In mature root tissues, the highest levels of CYCD2;1-GFP are detected in the nucleus of cells in LR meristems and the endodermis (arrows).

(I) to **(L)** *ProCYCD2;1:CYCD2;1-GFP* expression in LR founder cells and developing LR primordia.

(I) CYCD2;1-GFP in pericycle cell nuclei that migrated toward the common cell wall before initiation of the primordia (arrows).

(J) to **(L)** Stage II (staged according to Péret et al., 2009) primordia (**[J]** and **[K]**) and stage VIII **(L)** primordium. CYCD2;1-GFP accumulates in the nucleus of developing LR cells, but levels drop in the columella of emerged LRs (arrow). c, columella.
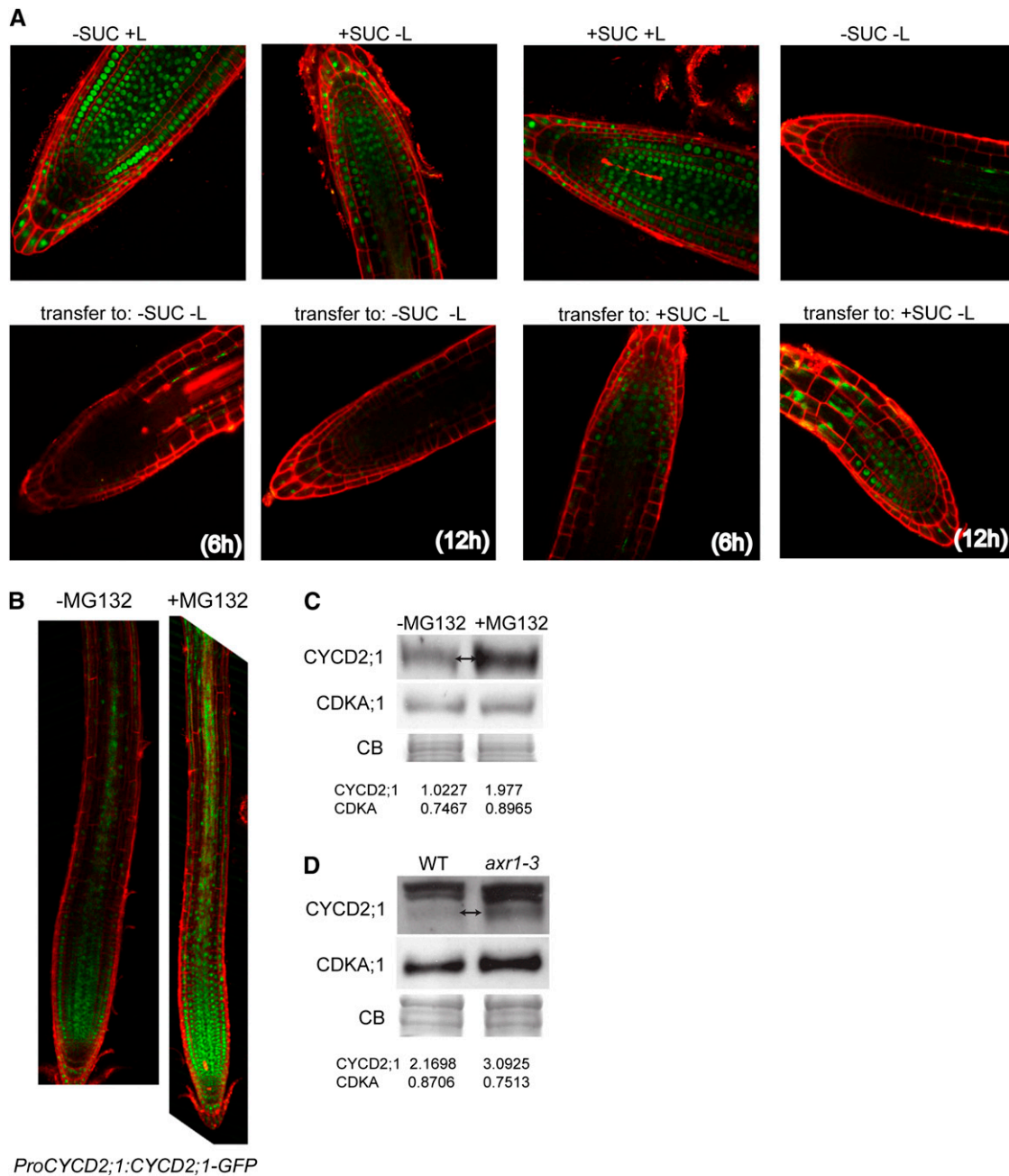
Figure 2. Regulation of CYCD2;1 Levels by Suc and Turnover by Proteasome-Mediated Degradation.

(A) Suc induces *ProCYCD2;1:CYCD2;1-GFP* expression in roots of dark-grown plants. Either light (L) or exogenous Suc (SUC) is sufficient for *ProCYCD2;1:CYCD2;1-GFP* expression in roots (top row). Seedlings grown in the dark on media lacking Suc for 5 d (top row, right panel) were transferred to media without (−SUC) or with (+SUC) in dark (−L) or light (+L) conditions and CYCD2;1-GFP was imaged after 6 and 12 h.
(B) to **(D)** Inhibition of proteasome activity increases CYCD2;1 accumulation.
(B) CYCD2;1-GFP accumulates in roots of 5-DAG *ProCYCD2;1:CYCD2;1-GFP* seedlings after 12 h of treatment with MG132, an inhibitor of the proteasome complex.
(C) Endogenous CYCD2;1 detected in a protein gel blot with anti-CYCD2;1 antiserum after 12 h of treatment of wild-type roots with MG132 (cf. bands indicated with the double arrow; values below the blots represent quantification relative to total signal in the loading control [CB]). CDKA;1 level detected with an anti-CDKA;1 antiserum is not changed (middle).
(D) CYCD2;1 levels are higher in the *axr1-3* mutant impaired in proteasome function. CDKA;1 levels and loading control (CB) are shown, which was used to estimate signal intensity (given below the blots). CB, Coomassie blue stain as loading control. WT, wild type.
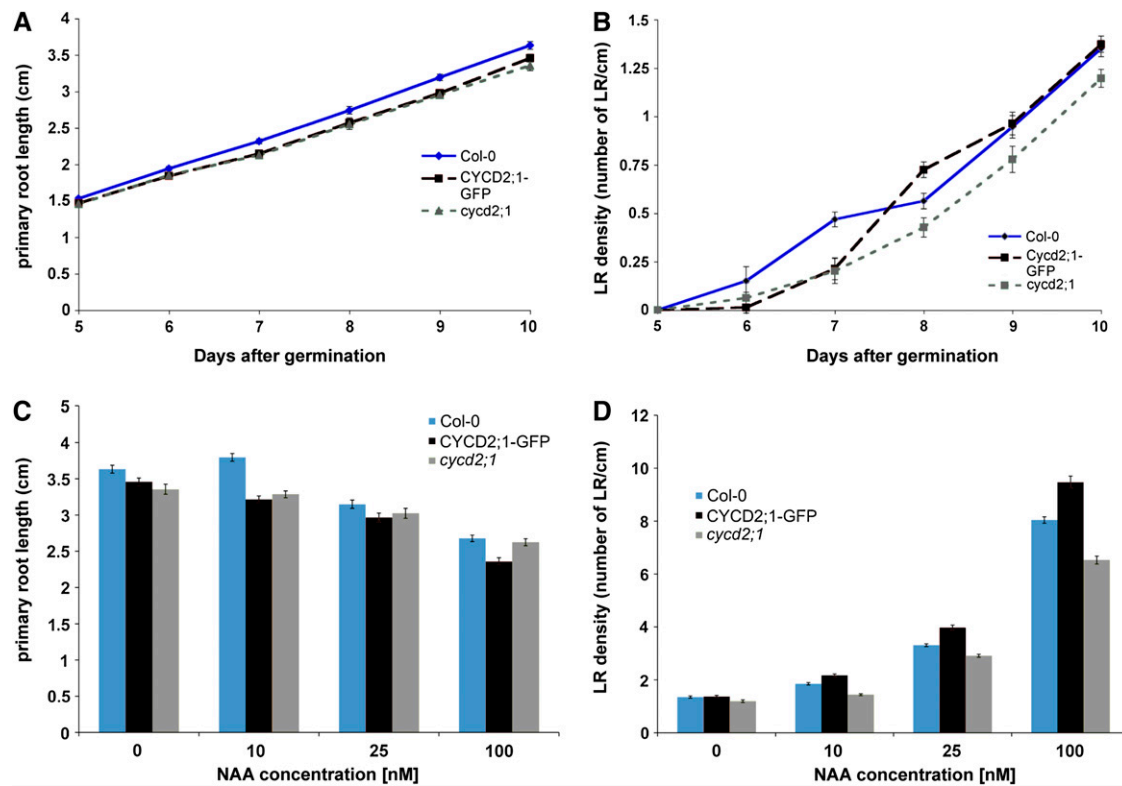
Figure 3. *CYCD2;1* Is Rate-Limiting for LR Induction by Auxin.

(A) and **(B)** Time course from days 5 to 10 of longitudinal primary root growth **(A)** and LR density **(B)** expressed as visible LRs per centimeter primary root of Col-0, *ProCYCD2;1:CYCD2;1-GFP*, and *cycd2;1* seedlings grown vertically under standard conditions in tissue culture shows only a minor difference in the LR density of *cycd2;1* compared with the wild type.

(C) and **(D)** Primary root length **(C)** and LR density **(D)** after 10 d of vertical growth on different NAA concentrations (0, 10, 25, and 100 nM) shows reduced LR auxin response in the *cycd2;1* mutant and increased response in the *ProCYCD2;1:CYCD2;1-GFP* line. Error bars represent SE; *n* = 30. [See online article for color version of this figure.]

levels (Wang et al., 1998; De Veylder et al., 2001; Cleary et al., 2002; Himanen et al., 2002; Verkest et al., 2005a). It has previously been reported that CYCD2;1 is able to interact with most of the ICKs/KRPs to differing extents in yeast two-hybrid assays (Zhou et al., 2002), making them likely candidates to regulate CYCD2;1 activity. Overexpression of the native *CYCD2;1* cDNA in *Arabidopsis* was previously reported to yield an aberrantly spliced mRNA, missing a portion of the conserved cyclin box essential for binding to CDKA (Qi and John, 2007). We investigated whether this also occurs in yeast and found that the expression of the *CYCD2;1* cDNA in *Saccharomyces cerevisiae* also yielded a shorter protein in addition to a protein of the expected size. Therefore, a non-spliceable variant of the *CYCD2;1* cDNA was generated (Qi and John, 2007) in the CYCD2;1-FL construct and used to analyze interactions with seven ICK/KRP proteins. In these yeast two-hybrid assays, using binding domain (BD)-CYCD2;1-FL and activation domain (AD)-ICK/KRP fusions, a spectrum of interactions was observed (Figure 4A). CYCD2;1 interacted most strongly with ICK2/KRP2 and to a moderate degree with ICK5/KRP7 and ICK7/KRP4. It showed possible weaker interaction with the other ICK/KRP proteins (ICK1/KRP1, ICK3/KRP5, ICK6/KRP3, and ICK4/KRP6).

We nevertheless note the previous reported interaction in planta between KRP1 and CYCD2;1 (Ren et al., 2008) and the interaction of CYCD2;1 with several ICK/KRPs in proteomic analysis (Van Leene et al., 2010). We also note that no interaction was detected in this yeast-based assay between full-length CYCD2;1 and CDKA (Figure 4B), in contrast with the coprecipitation of CYCD2;1 and CDKA in immunoprecipitation experiments from root extracts and cell suspensions (see Supplemental Figure 1C online; Healy et al., 2001). This, in combination with the interaction of ICK2/KRP2 with both CDKA;1 and CYCD2;1 in these yeast two-hybrid assays (Figure 4B), suggested a possible function for ICK2/KRP2 as a bridging factor enabling CDKs and CYCD2;1 to interact. Therefore, the interaction between the BD-CYCD2;1 and AD-CDK fusions in the presence and absence of ICK2/KRP2 was evaluated in the yeast system (Figure 4B), using the *LACZ* reporter and *HIS3* and *ADE* activity for positive selection. Introducing ICK2/KRP2 promoted the interaction between CYCD2;1 and CDKA;1, but not between CYCD2;1 and CDKB1;1, leading to the conclusion that ICK2/KRP2 is able to facilitate the interaction of CYCD2;1 and CDKA;1.
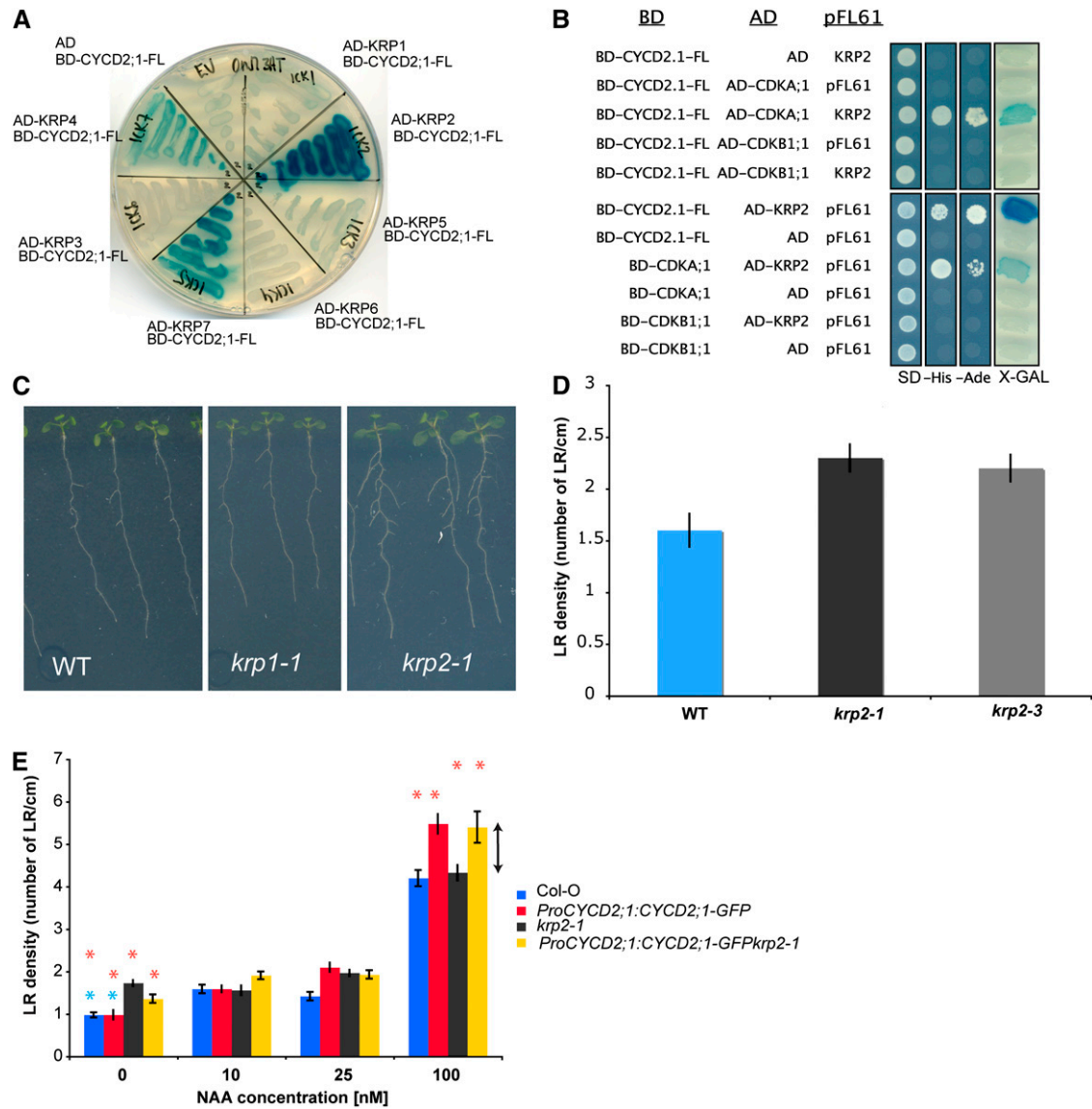
Figure 4. ICK2/KRP2 Promotes the Interaction between CYCD2;1 and CDKA;1 and Inhibits LR Formation.

(A) Yeast two-hybrid assays between CYCD2;1 and different ICK/KRP proteins. A modified *CYCD2;1* cDNA with a cryptic splice site removed (CYCD2;1-FL) (Qi and John, 2007) as a BD fusion was tested for interaction with various ICK/KRP proteins expressed as AD fusions or with the empty AD vector as a control. A strong interaction between CYCD2;1-FL and ICK2/KRP2 was detected, with the blue color indicating β-galactosidase activity after incubation with its substrate X-Gal.

(B) ICK2/KRP2 interacts with both CYCD2;1-FL and CDKA;1 and stimulates an interaction between CYCD2;1-FL and CDKA;1 in yeast three-hybrid assays. AD-ICK2/KRP2 interacts with both BD-CYCD2;1-FL and BD-CDKA;1 fusions, but not with BD-CDKB1;1. A strong interaction in these conditions between CYCD2;1-FL and CDKA;1 is detected only in the presence of ICK2/KRP2 but not upon transformation with the empty vector pFL61. Transformed yeast cells were grown on SD (dropout) medium lacking Leu, Trp, and uracil, and the interaction was scored visually by determining yeast growth on this same medium lacking either His (−His) or either adenine (−Ade) or by the appearance of a blue reaction product from β-galactosidase activity.

(C) Root systems of the wild type (WT), *krp1-1*, and *krp2-1* mutants 10 DAG.

(D) LR density (LRs/cm primary root) in 9-DAG wild type (left), *krp2-1* (center), and *krp2-3* (right) mutants. Bars represent SE; *n* = 30.

(E) Quantification of LR density in Col-0, *ProCYCD2;1:CYCD2;1-GFP*, *krp2-1*, and *ProCYCD2;1:CYCD2;1-GFP krp2-1* lines treated with 0, 10, 25, or 100 nM NAA. Increased LR density is observed in lines with the *krp2-1* mutation when grown without additional auxin compared with lines wild-type for *ICK2/KRP2*. Blue star, not significant; red star, significant difference (95% confidence interval). Seedlings grown on 100 nM NAA show increased LR density in the presence of *ProCYCD2;1:CYCD2;1-GFP* (double-headed arrows). Error bars indicate SE; *n* = 30.

[See online article for color version of this figure.]

We also investigated whether the splice variant CYCD2;1 protein lacking the cyclin box (CYCD2;1-TR) can interact with ICK2/KRP2 or CDKA;1 in yeast and found no evidence for an interaction of this truncated CYCD2;1 variant with either ICK2/KRP2 or CDKA;1 (see Supplemental Figure 1D online).

KRP2 Inhibits Lateral Root Formation

Elevating either ICK1/KRP1 or ICK2/KRP2 levels blocks lateral root initiation and counteracts the stimulation of lateral roots by auxin (Himanen et al., 2002; Ren et al., 2008). Conversely, when concentrated auxin treatment was used to reactivate the pericycle in naphthylphthalamic acid (NPA) pretreated roots, *ICK1/KRP1*, *ICK2/KRP2*, and *KRP4/ICK7* transcript levels were reduced, whereas *KRP3/ICK6* was induced (Himanen et al., 2002).

To investigate further the role of these *ICK/KRP*s genes in the formation of lateral roots, we screened insertion mutant lines for *ick1/krp1* and *ick2/krp2* for effects on lateral root numbers (Figure 4C). One allele of *ick1/krp1* (*krp1-1*) (see Supplemental Figure 2A online) and two independent alleles of *ick2/krp2* (*krp2-1* and *krp2-3*) (see Supplemental Figure 1E online) were identified, and all three were confirmed to have lost full-length *ICK1/KRP1* and *ICK2/KRP2* transcripts, respectively. *krp2-1* was characterized by the absence of 5′ transcript with respect to the T-DNA and in *krp2-3* no 3′ transcripts could be detected. After a visual screen, scoring the emerged lateral roots in the *ick2/krp2* mutants after 9 d confirmed that both *ick2/krp2* mutant alleles had an increased number and density of lateral roots under standard conditions (Figure 4D; 40% increase compared with the wild type, P < 0.002), revealing that *ICK2/KRP2* has an inhibitory effect on lateral root density. Both mutant alleles had a similarly elevated lateral root density (P = 0.75). In a separate set of experiments, loss of *ICK2/KRP2* stimulated lateral root density to the equivalent frequency as that observed when wild-type roots were treated with 10 nM NAA (Figure 4E), at which concentration and above the stimulatory effect of the *ick2/krp2* mutation was lost. Hence, upon treatment with 100 nM NAA, the lateral root density is upregulated in the *krp2-1* mutant to the same extent as in the wild type, indicating that at higher auxin concentrations the presence of a functional *ICK2/KRP2* gene is no longer inhibitory (Figure 4E).

Interestingly, in the absence of auxin, lateral root (LR) density was increased in the *krp2-1 ProCYCD2;1:CYCD2;1-GFP* line (red star, average *ProCYCD2;1:CYCD2;1-GFP* emerged LR density = 0.98 LR/cm; average *ProCYCD2;1:CYCD2;1-GFP krp2-1* emerged LR density = 1.36 LR/cm, 37% increase, P = 0.0005), consistent with *krp2-1* exhibiting a partially constitutive auxin response (Figure 4E). As noted before (Figure 3D), *ProCYCD2;1:CYCD2;1-GFP* did not have an effect in the wild-type background under standard conditions (Figure 4E, blue star, average wild-type density 0.98 LR/cm, average *ProCYCD2;1:CYCD2;1-GFP* density 0.98 LR/cm, 0% increase, P = 0.49) but did increase LR density at higher auxin concentrations. When the *ProCYCD2;1:CYCD2;1-GFP* fusion and *ProCYCD2;1:CYCD2;1-GFP krp2-1* lines were grown on 100 nM auxin, LR formation was stimulated to a similar level in both wild-type (P = 0.003, comparing Columbia-0 [Col-0] and *ProCYCD2;1:CYCD2;1-GFP*) and *krp2-1* (P = 0.014, evaluating *krp2-1* and

ProCYCD2;1:CYCD2;1-GFP krp2-1) backgrounds, showing again that LR density under auxin stimulation is independent of ICK2/KRP2 presence (Figure 4E, double arrow) but responds to CYCD2;1 level.

KRP2 Levels Are Regulated by Auxin

LR density in both the wild type and the *ick2/krp2* mutants responded to 100 nM NAA to the same extent, suggesting that auxin could modulate levels of ICK2/KRP2 (Figure 4E). We therefore examined whether auxin could restore LR formation in the *35S:ICK2/KRP2-GFP* line constitutively overexpressing *ICK2/KRP2*. Under standard conditions without added auxin, constitutive *ICK2/KRP2-GFP* overexpression inhibited LR initiation almost completely (Figures 5A, top panels, and 5B), while it reduced the length of the primary root by half (Figure 5C). Twelve DAG, few *35S:ICK2/KRP2-GFP* seedlings displayed LRs (Figure 5B). However, when grown on 100 nM auxin, *35S:ICK2/KRP2-GFP Arabidopsis* seedlings displayed on average 0.2 LRs/mm primary root after 12 d (Figures 5A, bottom panels, and 5D), the same density as found in untreated wild-type seedlings. In the wild type, supplementing the medium with 100 nM auxin doubled the LR density. We obtained comparable results when treating the *35S:ICK1/KRP1* line (Ren et al., 2008) with 10 and 100 nM NAA, indicating that auxin treatment can overcome the inhibition of LR initiation observed upon *ICK1/KRP1* or *ICK2/KRP2* overexpression.

To establish whether this rescue of LR formation by auxin involved the reduction of the ICK2/KRP2 protein levels, we analyzed by immunoblot analysis the ICK2/KRP2-GFP levels in roots of the *35S:ICK2/KRP2-GFP* line 24 h after transfer of 5 DAG seedlings to media with increasing auxin concentrations (Figure 5E). We observed an inverse correlation between the NAA concentration in the growth medium and levels of ICK2/KRP2-GFP in the *35S:ICK2/KRP2-GFP* line, leading us to conclude that auxin affects the levels of ICK2/KRP2-GFP protein (Figure 5E).

A single nuclear localization domain is responsible for the nuclear localization of ICK2/KRP2 (Bird et al., 2007). In *ProKRP2:KRP2-GFP* lines, we could detect ICK2/KRP2-GFP in the nuclei of older tissues, and in the LR cap, but levels were below detection in the RAM (Figure 5F). Similarly, 35S promoter–driven ICK2/KRP2-GFP could be detected in the nucleus in elongated root tissues above the RAM, in the LR cap, and in the differentiated columella cells, but ICK2/KRP2-GFP fluorescence was weaker and more dispersed in the cells of the RAM, the columella stem cells, and the less differentiated cells of the columella (Figure 5F). This suggests that ICK2/KRP2 levels and cellular distribution are differentially controlled in the different root tissues and tightly regulated in the RAM. Auxin treatment of the constitutive ICK2/KRP2-GFP OE line induced root primordia (Figure 5G, bottom panel) and reduced ICK2/KRP2-GFP fluorescence intensity particularly in the endodermis, pericycle, and vascular tissues (Figure 5G, middle versus top panel) in mature tissues. Since auxin is capable of reducing the effect of constitutive *ICK2/KRP2* overexpression by lowering ICK2/KRP2 protein levels, we conclude that ICK2/KRP2 levels are posttranscriptionally regulated by auxin.
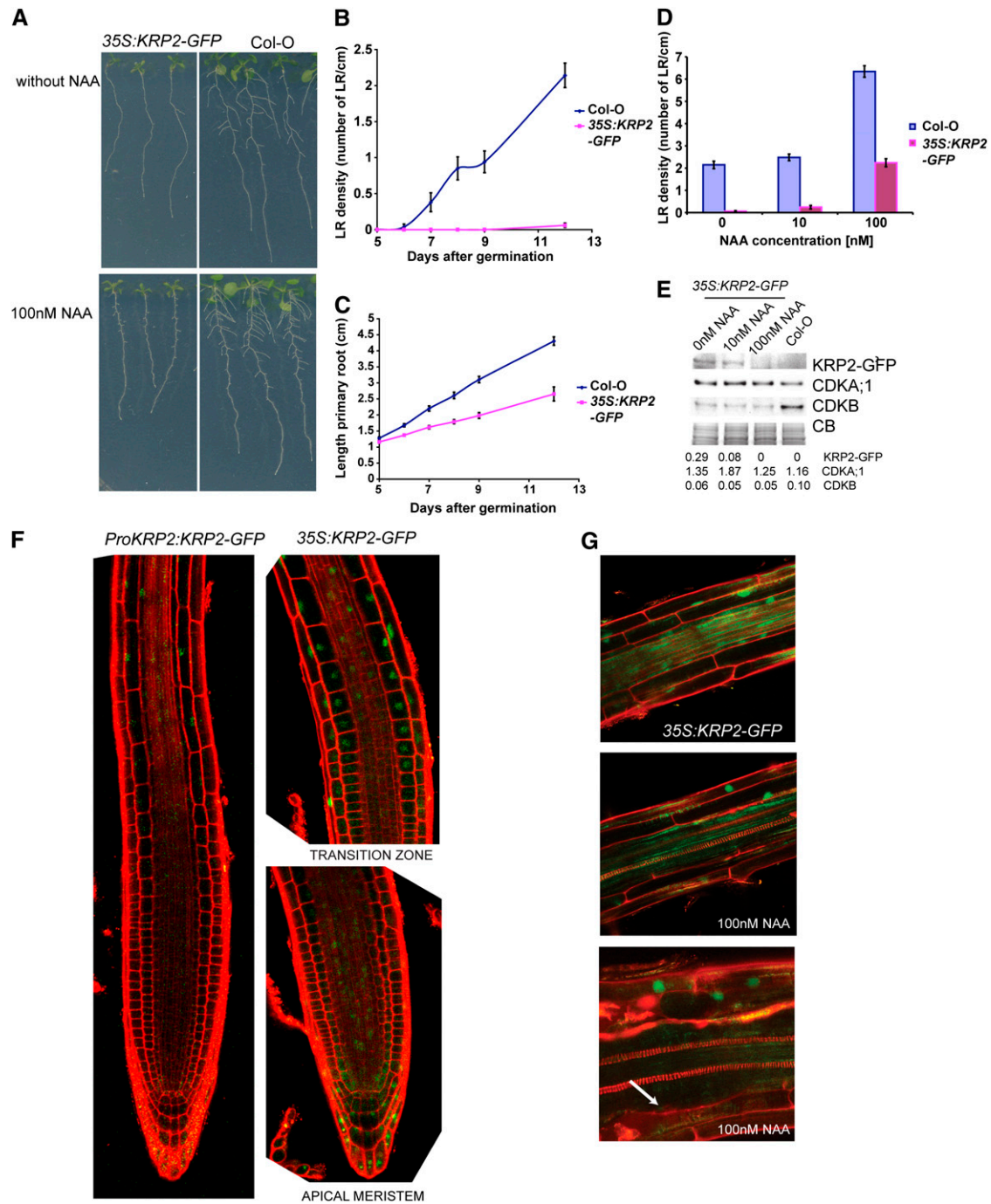
Figure 5. Auxin Reduces ICK2/KRP2 Levels and Rescues the LR Inhibition Caused by *ICK2/KRP2* Overexpression.

(A) Auxin treatment (100 nM NAA; bottom panels) partially restores LR formation to *35S:ICK2/KRP2-GFP* seedlings (left panels). Wild-type (Col-0) seedlings are shown on the right.

(B) and **(C)** *ICK2/KRP2* overexpression inhibits LR density **(B)** to a greater extent than primary root growth **(C)**.

(D) LR density (LRs/cm primary root) in *35S:KRP2-GFP* (right bar in each pair) and wild-type (left bar) seedlings grown in presence of 0, 10, or 100 nM NAA.

(E) Protein gel blot analysis with anti-GFP (top), anti-CDKA;1 (second row), and anti-CDKB antisera. Extracts were prepared from roots 24 h after transfer to media containing the indicated auxin concentrations. CB, Coomassie blue–stained loading control used to calculate background corrected ratios (listed below blot).

(F) ICK2/KRP2-GFP localization; expression under control of the native promoter sequence (left) or 35S (right). ICK2/KRP2-GFP accumulates in the nucleus of elongated tissues and in the outer root cap cells, while it has lower levels in the meristem and in the columella stem cells.

(G) *35S:ICK2/KRP2-GFP* roots treated with 100 nM NAA (middle and bottom) show that LR formation is induced in the pericycle with concomitant reduction in ICK2/KRP2-GFP signal in the primordium (arrow).

KRP2 Affects the Subcellular Localization of CYCD2;1

Since CYCD2;1 was found to accumulate in the nuclei of cells in the root meristem and vascular tissues (Figure 6A, first panel), two prediction tools (PredictNLS, https://rostlab.org/owiki/index.php/PredictNLS; and PSort, http://psort.hgc.jp/) were used to search for nuclear targeting information within the amino acid sequence of CYCD2;1. No consensus nuclear localization signal was found in CYCD2;1 using these algorithms. ICK1/KRP1 coprecipitated with CYCD2;1 in extracts (see Supplemental Figure 1C online; Ren et al., 2008) and since both ICK1/KRP1 and ICK2/KRP2 are reported to be localized in the nucleus (Bird et al., 2007), we investigated whether these KRPs could affect the subcellular localization of CYCD2;1. For this purpose, the *ProCYCD2;1:CYCD2;1-GFP* construct was crossed into the *krp2-1* and *krp1-1* backgrounds. CYCD2;1-GFP was exclusively cytoplasmic and excluded from the nucleus in root cells in the *ick2/krp2* mutant background (Figure 6A, second panel) but retained its wild-type intracellular distribution in *ick1/krp1* (Figure 6A, third panel). However, CYCD2;1 is not required for the nuclear localization of ICK2/KRP2, since ICK2/KRP2-GFP still decorated the nuclei in the *cycd2;1* mutant background (Figure 6A, fourth panel) in the same tissues as in the wild type (Figure 5F). Modulating levels of ICK2/KRP2 may influence CYCD2;1 levels, since immunoblot analysis of CYCD2;1-GFP levels in roots of *ick2/krp2* (Figure 6B; see Supplemental Figure 3 online) and in the *ICK2/KRP2* OE (Figure 6C; see Supplemental Figure 3 online) backgrounds revealed slightly reduced levels in both cases compared with the wild type, but they nevertheless indicate that CYCD2;1-GFP is still present in both cases, supporting the confocal microscopy observations. Taken together, these observations demonstrate that ICK2/KRP2 can influence the nuclear localization of CYCD2;1.

The Auxin Response Affects Levels of ICK2/KRP2 and Intracellular Location of CYCD2;1

CYCD2;1 intracellular distribution was noted to be less nuclear focused in columella cells of the root cap (Figure 7A), which are characterized by a strong activation of the artificial *DR5* auxin response reporter (Figure 7A, top left) (Sabatini et al., 1999), despite a low auxin content (Petersson et al., 2009). This led us to test whether auxin response could influence the nuclear localization of CYCD2;1. Successive treatments with an auxin transport inhibitor (NPA) and exogenous auxin (NAA) were used (Himanen et al., 2002) to modulate the sites of *DR5* auxin response. Growing seedlings on NPA expanded the expression domain of *DR5:GFP* and activated the *DR5:GFP* auxin reporter in the LR cap (Figure 7A, top middle panel, arrow). Whereas subsequent treatment with NAA did not increase overall CYCD2;1 protein levels in NPA-grown plants and does not elevate *CYCD2;1* expression or protein levels in control seedlings (see Supplemental Figures 1A, 1B, and 1F online), it led to activation of an auxin response in the basal meristem, as well as an auxin response in the quiescent center and root cap, as revealed by the activation of the *DR5:GFP* reporter in these regions (Figure 7A, top right, arrows). When *ProCYCD2;1: CYCD2;1-GFP* seedlings were grown on standard medium (Figure 7A) or medium supplemented with NPA (Figure 7A, left and middle panels), nuclear CYCD2;1-GFP signal was detected in the nuclei

of most cells of the primary meristem and in pericycle cells of the elongation differentiation zone. Independent of the presence of NPA, the nuclei of columella stem cells were devoid of nuclear CYCD2;1-GFP (Figure 7A). The NPA treatment, which expanded the *DR5:GFP* reporter activity into the LR cap, concomitantly reduced the nuclear CYCD2;1-GFP signal in the cells of the LR cap (Figure 7A, middle panels), consistent with an increased auxin response in these cells affecting ICK2/KRP2 protein levels and hence influencing CYCD2;1 nuclear localization. Subsequent treatment with auxin led to a reduced CYCD2;1-GFP signal in the nuclei of cells of the basal meristem (Figure 7A, bottom right) together with an increased *DR5:GFP* signal, and this effect was particularly prominent in the vasculature. Plants grown on NPA have an increased CYCD2;1-GPF protein level in roots, but transfer to NAA-containing media restores the CYCD2-GFP level to that of untreated roots (Figure 7A, second row; see Supplemental Figure 1F online).

To verify if ICK2/KRP2 levels also are affected by local activation of the auxin response, we performed the experiment on *35S:KRP2-GFP* seedlings. However, we found that *35S:KRP2-GFP* seedlings failed to develop on NPA in our culture conditions, so instead of growing seedlings on NPA, 5-DAG *35S:KRP2-GFP* and *DR5:GFP* auxin response reporter seedlings were transferred to NPA-supplemented medium. Forty hours after transfer, the *DR5* reporter expression extended into the LR cap (Figure 7B), which coincided with a drop in KRP2-GFP fluorescence.

From these results, we conclude that there is an inverse correlation between auxin response and the nuclear localization of CYCD2;1, consistent with auxin-mediated downregulation of ICK2/KRP2 levels influencing the amount of nuclear localized CYCD2;1.

CYCD2;1 Becomes Rate-Limiting for LR Formation When ICK2/KRP2 Is Absent or Destroyed

To establish the genetic interaction between *CYCD2;1* and *ICK2/KRP2* in LR density, we compared LR formation in the *cycd2;1 krp2-1* double mutant, *krp2-1* and *cycd2;1* single mutants, and the wild type (Figure 7C). When growing on media without auxin, additional loss of *CYCD2;1* function in the *ick2/krp2* background reverted the elevated LR phenotype of the single *krp2-1* mutant: the LR density of the *krp2-1 cycd2;1* double mutant was not significantly different from the wild type (P = 0.29) or the *cycd2;1* mutant (P = 0.45), whereas the *krp2-1* mutant had elevated levels when compared with the wild type (P = 0.0071), *cycd2;1* (P = 0.011), and *cycd2;1krp2-1* (P = 0.038). Hence, the increased LR frequency seen in the *krp2-1* mutant depends on a functional *CYCD2;1* gene.

In the presence of 25 nM NAA, the auxin response of *cycd2;1* mutants was reduced (Figure 3D) and that of *krp2-1* mutants was slightly increased (Figure 4E). These results are supported by this new experiment, confirming both that CYCD2;1 levels are rate-limiting under auxin-stimulated conditions and the genetic epistasis between *ICK2/KRP2* and *CYCD2;1.*

ICK2/KRP2- and CYCD2;1-Associated Alterations in LR Density Are Not Linked to Changes in the Basal Meristem

We have previously shown that Suc-responsive changes in LR density depend on the presence of an intact *CYCD4;1* gene and
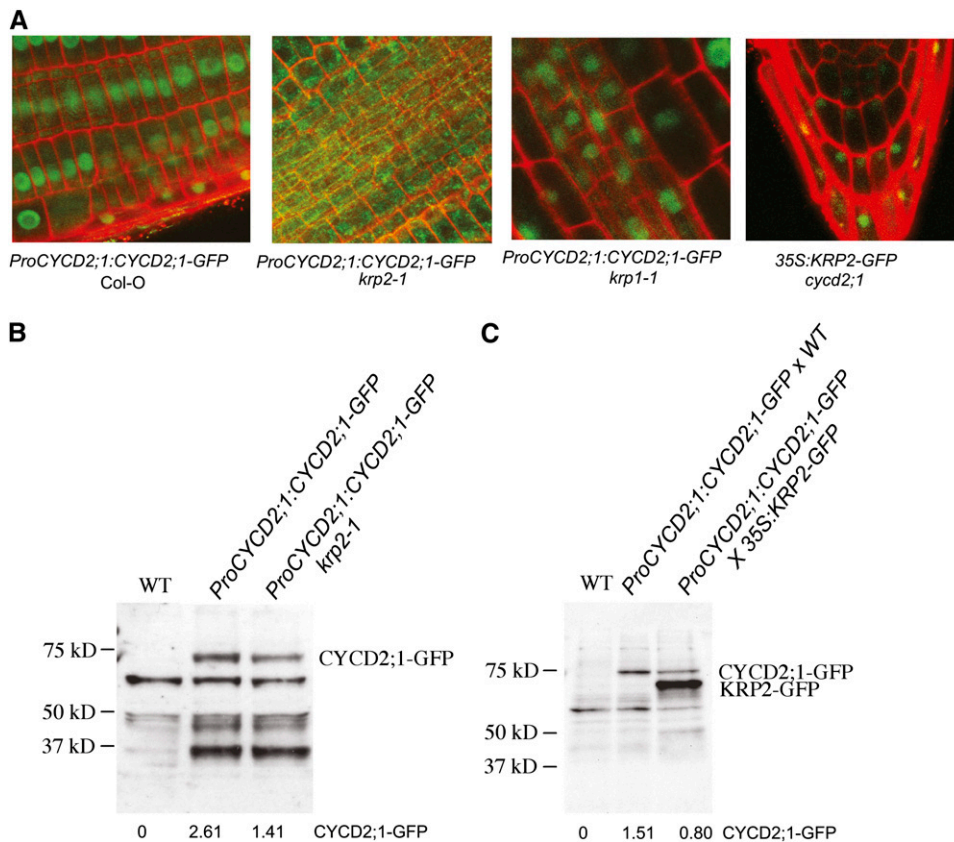
A

ProCYCD2;1:CYCD2;1-GFP
Col-O

ProCYCD2;1:CYCD2;1-GFP
krp2-1

ProCYCD2;1:CYCD2;1-GFP
krp1-1

35S:KRP2-GFP
cycd2;1

Figure 6. CYCD2;1 Cellular Distribution Is Modulated by ICK2/KRP2.

(A) Nuclear accumulation of CYCD2;1-GFP in the wild-type Col background (left) compared with primarily cytoplasmic localization of CYCD2;1-GFP in the *krp2-1* background (center left). CYCD2;1-GFP remains nuclear in the *krp1-1* mutant (center right). By contrast, ICK2/KRP2-GFP does not require CYCD2;1 function for its nuclear localization (*35S:ICK2/KRP2-GFP* in *cycd2;1*, right; compare with Figures 5F and 5G).

(B) Protein gel blot analysis using anti-CYCD2;1 antiserum of the wild type (WT; left lane), *ProCYCD2;1:CYCD2;1-GFP* (center lane), and *ProCYCD2;1: CYCD2;1-GFP* (right lane) in the *ick2/krp2* mutant. CYCD2;1-GFP levels are slightly reduced in *krp2-1*. The relative intensity of background corrected signal for CYCD2;1-GFP is shown below. Loading controls are shown in Supplemental Figure 3 online.

(C) Protein gel blot using anti-GFP antiserum of the wild type (left lane), hemizygous *ProCYCD2;1:CYCD2;1-GFP* × wild type (center), and *ProCYCD2;1: CYCD2;1-GFP* × 35S:ICK2/KRP2-GFP (right). The relative intensity of background corrected signal for CYCD2;1-GFP is shown below.

are linked to changes in cell size in the basal meristem region (Nieuwland et al., 2009). We therefore examined basal meristem cell size in wild-type, *cycd2-1*, and *krp2-1* roots grown in standard conditions and in the presence of 25 nM NAA (see Supplemental Figure 4B online). In a separate experiment, we compared cell sizes across the entire apical and distal meristems in wild-type, *krp2-1*, and *krp2-3* roots (see Supplemental Figure 4A online). Unlike the situation in *cycd4;1* mutants, we observed no systematic differences in cell sizes between the different genetic backgrounds, nor depending on auxin concentration. We therefore conclude that neither the LR response to 25 nM NAA nor the mechanism mediated by *CYCD2;1* and *ICK2/KRP2* are linked to distal meristem cell size differences.

DISCUSSION

Three principal types of growth occur in the *Arabidopsis* root. Longitudinal growth derives ultimately from the new cells produced as a consequence of cell division in the primary apical meristem (RAM). Secondary radial growth arising from cambial activity leads to the thickening of the older root. Finally, root branching occurs as a result of pericycle cells outside the primary meristem resuming division to initiate LRs. LRs appear to be prepatterned in the pericycle cell layer within the region of the meristem in which cell division is slowing and average cell size is increasing, known as the basal meristem, due to periodic fluctuations in auxin or gene expression (De Smet et al., 2007; Nieuwland et al., 2009; Moreno-Risueno et al., 2010). A second auxin-dependent signal is then required to trigger the actual initiation process in pericycle cells adjacent to the xylem axis within the root hair differentiation zone (Péret et al., 2009), in which the *IAA14-ARF7/9* pathway is involved. LRs can also be triggered by the auxin maxima created by mechanical root bending or gravitropic signals (Ditengou et al., 2008; Laskowski et al., 2008; Richter et al., 2009).
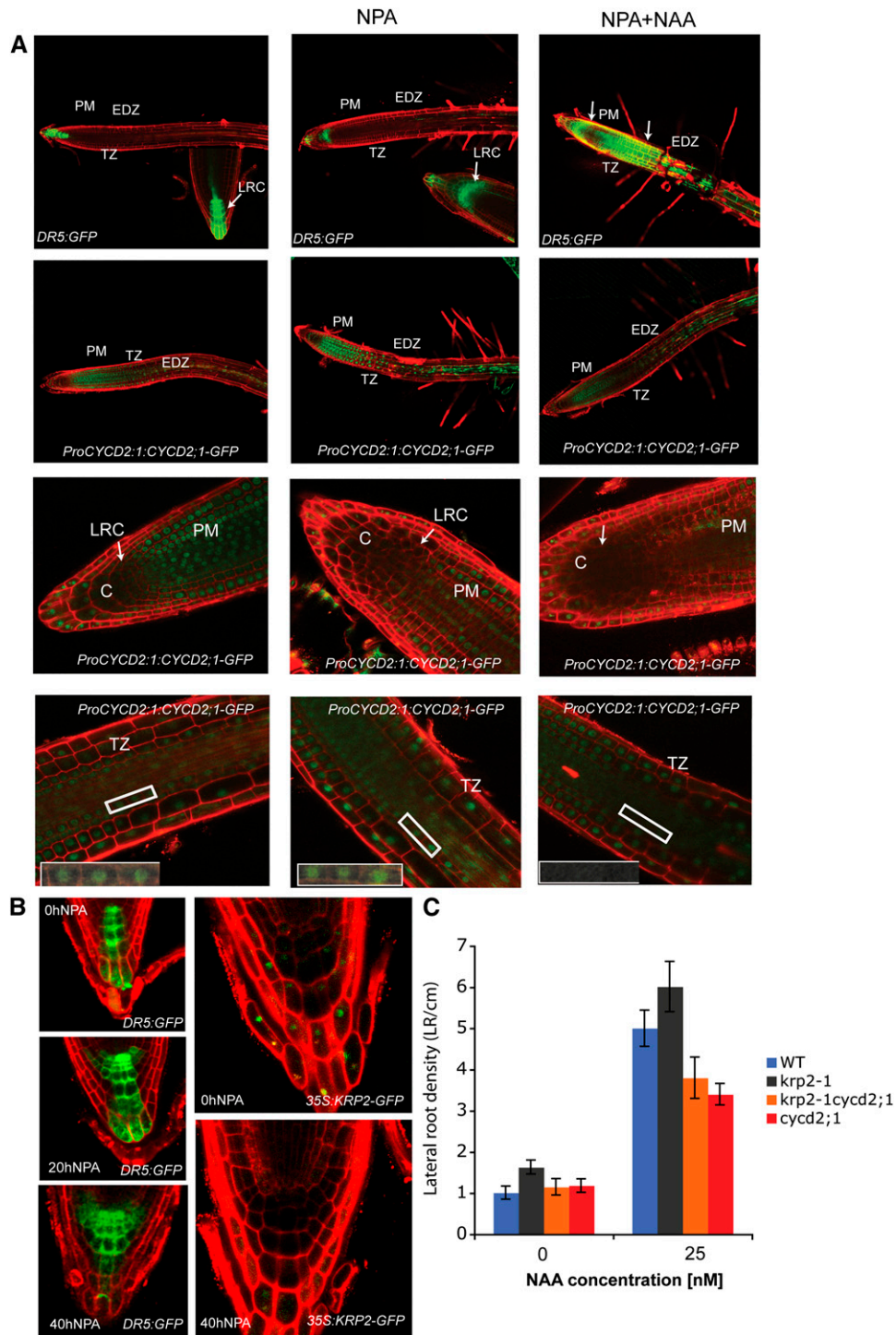
Figure 7. Auxin Response Modulates Intracellular CYCD2;1 Localization and KRP2 Levels, and CYCD2;1 Is Required for the *ick2/krp2* Phenotype.

(A) Detection of *DR5:GFP* auxin response reporter (top row) and *ProCYCD2;1:CYCD2;1-GFP* (bottom rows) in roots that were untreated (left panels), NPA grown (NPA; center), or NPA grown and then transferred to NAA for 24 h (NPA + NAA; right). Row 2, overall view of rot tip; row 3, apical meristem; row 4, transition zone (TZ). Boxes demarcate region shown enlarged in inset. NPA treatment induces the *DR5:GFP* auxin response reporter in the LR cap, and NPA followed by NAA induces *DR5:GFP* in both transition zone and LR cap (top panels). In regions where the *DR5:GFP* reporter is activated by the NPA or combined NPA and NAA treatment, nuclear CYCD2;1-GFP is reduced (arrows). LRC, lateral root cap; PM, primary meristem; C, columella; TZ, transition zone; EDZ, elongated differentiation zone.

These data imply that specific root tissues outside the RAM maintain the capacity to respond to mitogenic signals that induce division. In the case of LR formation, the major signal is auxin (Fukaki et al., 2002; De Smet et al., 2007; Okushima et al., 2007; Laskowski et al., 2008), which therefore must ultimately impinge on cell cycle control. Although transcript profiles in *Arabidopsis* roots have been analyzed during synchronized LR initiation (Himanen et al., 2002, 2004), the molecular mechanisms at the interface of the cell cycle that allow pericycle cells to be responsive to signaling and potentiate LR priming and the consequent divisions are not well understood. Our data associate CYCD2;1 and its interacting protein ICK2/KRP2 with this process.

Several lines of experimental evidence indicate important roles for CYCD in regulating cell division (De Veylder et al., 2002; Schnittger et al., 2002; Dewitte et al., 2003, 2007; Ebel et al., 2004; Wildwater et al., 2005; Qi and John, 2007). *CYCD3* genes promote cell proliferation in leaf tissues and delay the onset of cell elongation and associated endoreduplication, and loss-of-function mutants have the inverse phenotype (Dewitte et al., 2003, 2007). Enhanced *CYCD3;1* levels stimulate proliferation of the stem cell population of the columella (Wildwater et al., 2005), and overexpression of *CYCD2;1* promotes cell division in the RAM (Qi and John, 2007). Loss of *CYCD4;1* function in the pericycle confers premature elongation of cells located in the basal root meristem, indicative of a reduced probability for cell division and loss of Suc responsiveness in LR density, presumably by affecting the prepatterning process (Nieuwland et al., 2009).

Increasing levels of G_1/S regulators, such as by 35S-driven overexpression of *CYCD3;1* and the heterodimeric *E2Fa/DPa* transcription factor, enhanced the response of pericycle cells toward auxin but appeared unable to stimulate pericycle cells under standard conditions (De Smet et al., 2010), indicating that stimulating the cell cycle under specific conditions has the potential to promote LR development. The analysis of the role of *CYCD2;1* in LR density leads us to a model in which CYCD2;1 activity contributes to normal responses to auxin in modulating LR density (Figure 8). We suggest that CYCD2;1 is involved in a two-step manner. In the first step, CYCD2;1 becomes nuclear localized in a process involving interaction with ICK2/KRP2, based on the failure to detect nuclear CYCD2;1-GFP in the *krp2-1* mutant background. We suggest that this nuclear accumulation of CYCD2;1-ICK2/KRP2 leads to a reservoir of preformed nuclear CYCD2;1-ICK2/KRP2-CDKA kinase complexes that can be activated by auxin-mediated downregulation of ICK2/KRP2 (Figure 8). We note that the uptake of CDKA into the nucleus as a consequence of ICK1/KRP1 association has been demonstrated (Zhou et al., 2006). Formally we do not know if the proposed nuclear accumulation of CYCD2;1-ICK2/KRP2 involves CDKA in the same

complex. However, given the capacity of ICK2/KRP2 to act as a bridging factor for CYCD2;1 to interact with CDKA;1 and the coimmunoprecipitation of CDKA;1 with CYCD2;1, this seems a likely scenario.

The CYCD2;1 protein normally located in the nucleus presumably remains inactive until the inhibition imposed by ICK2/KRP2 is removed. Since we find that ICK2/KRP2 levels are posttranscriptionally responsive to auxin, and Himanen et al. (2002) have previously shown evidence for transcriptional regulation, the initiation of LRs by an auxin pulse would result both in the reduction of *ICK2/KRP2* expression and the targeted turnover of ICK2/KRP2 protein, allowing CYCD2;1-containing CDK complexes to become activated in the second step and initiate cell division. The positive effect of mitotic CDKB-mediated ICK2/KRP2 phosphorylation on ICK2/KRP2 proteolysis (Verkest et al., 2005b) could amplify this effect triggered by auxin as the cell cycle initiates. We therefore propose that the auxin response modulates the activity of CYCD2;1 posttranscriptionally by affecting the levels of ICK2/KRP2 in specific tissues (Figure 8).

A number of lines of evidence presented here are consistent with this model. In standard conditions, LR density is similar for wild-type, *cycd2;1*, and moderately overexpressing *Pro-CYCD2;1:CYCD2;1-GFP* lines, although possibly slightly reduced in *cycd2;1* mutants, suggesting that CYCD2;1 activity is normally constrained by the inhibiting action of ICK2/KRP2. As auxin levels increase, *ICK2/KRP2* expression reduces and ICK2/KRP2 protein turnover is promoted, and levels of CYCD2;1 therefore become rate-limiting. Hence, a lower LR density is observed in *cycd2;1* mutants and a high density in the *Pro-CYCD2;1:CYCD2;1-GFP* line in the presence of ectopic auxin. Moreover, in the *ick2/krp2* mutant background, LR density in the absence of added auxin is similar to the wild type treated with 10 to 25 nM NAA, consistent with the effect in the wild type being due to ICK2/KRP2 turnover by auxin. Comparison of the *krp2-1* mutant with the *krp2-1 cycd2;1* double mutant in different auxin regimes shows that *cycd2;1* is epistatic to *ick2/krp2*. Hence, *CYCD2;1* is required for the elevated LR density of the *ick2/krp2* phenotype.

Several aspects of CYCD2;1 action remain unresolved. First, we cannot determine the point of action of CYCD2;1. An attractive possibility is that CYCD2;1 complexes form and become nuclear in the basal meristem where it is proposed that LR primordia are prepatterned and that these preformed complexes are then maintained until LR initiation is triggered in the *AUX/IAA14/SLR*-dependent process in the initiation zone. We have previously shown that a change in cell size in the basal meristem in mutants of the related *CYCD* gene *CYCD4;1* leads to a reduction in LR density, a phenotype that is restored by low concentrations of ectopic auxin (Nieuwland et al., 2009). The

---

Figure 7. (continued).

(B) *DR5:GFP* expression before and after 20 and 40 h. Transfer to NPA for 40 h extends *DR5:GFP* expression in the LR cap (left panels), coinciding with a drop of *35S:KRP2-GFP* expression (right panels).

(C) LR density of indicated genotypes in standard conditions and in presence of 25 nM NAA. On media without auxin, loss of *CYCD2;1* function reverts the *krp2-1* phenotype, reducing the *krp2-1* LR density to wild-type (WT) density. On auxin, CYCD2;1 is a rate-limiting factor for LR induction, as both *cycd2;1* and *krp2-1 cycd2;1* display reduced stimulation by 25 nM NAA. Error bars represent SE; *n* = 30.
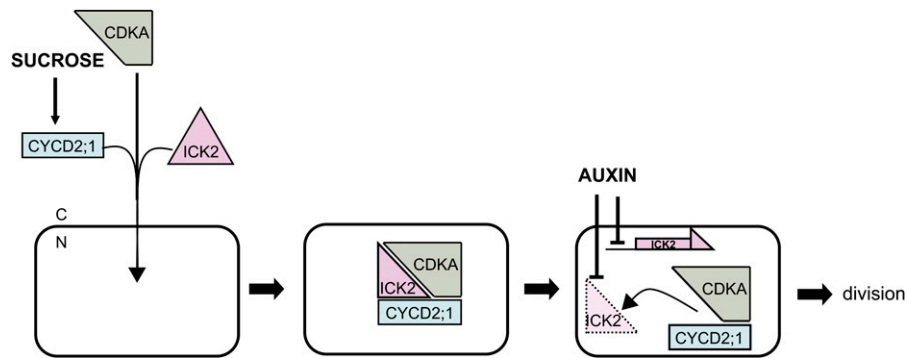
Figure 8. Model of Regulation of CYCD2;1 Activity by ICK2/KRP2 in Roots.

Suc stimulates *CYCD2;1* transcription, and we propose that the association of CYCD2;1 with ICK2/KRP2 is involved in nuclear accumulation of CYCD2;1 complexes (left), resulting in preformed but inactive complexes of CDKA, CYCD2;1, and ICK2/KRP2 in the nucleus (center). Auxin inhibits both ICK2/KRP2 gene expression and increases ICK2/KRP2 protein turnover, which leads to a transient increase in nuclear CYCD2;1-CDKA activity (right), which enhances the potential for cell division. N, nucleus; C, cytoplasm.
[See online article for color version of this figure.]

response of LR density to Suc also appears to involve cell size changes in this region (Nieuwland et al., 2009). However, we could detect no correlative change of cell length in the basal meristem region with LR density in *cycd2;1* or *ick2/krp2* mutants grown with or without 25 nM supplementary auxin (see Supplemental Figure 4 online). Moreover, cell size in the basal meristem of wild-type roots does not change in the presence of 25 nM auxin, although this is sufficient to promote an increase in LR density, suggesting that auxin does not exert its effect through the same mechanism as Suc in this region. We therefore propose that CYCD2;1 complexes are most likely to have their role in the auxin and *AUX/IAA14/SLR*-dependent induction of LR primordia or in an aspect of prepatterning that is independent of basal meristem cell size.

We examined the spatiotemporal distribution of transcripts derived from profiling sorted root cells from different tissues (Brady et al., 2007) by means of the eFP browser (http://bar.utoronto.ca/efp/cgi-bin/efpWeb.cgi; Winter et al., 2007), but this does not provide clear evidence as to the possible point of action of *CYCD2;1* and *ICK2/KRP2*. The data indicate that *CYCD2;1* transcripts are highest in the RAM, especially in the pericycle and endodermis cells adjacent to the xylem poles. We observed the distribution of CYCD2;1-GFP protein broadly in agreement with this. In older root tissues, the highest concentration of *CYCD2;1* transcripts is still detected in the endodermis and pericycle, with a maximum at the pericycle poles, albeit it a lower level. According to Brady et al. (2007), *CDKA;1* transcripts maintain their highest levels in the pericycle cells adjacent to the xylem poles in mature root tissues. Levels of *ICK2/KRP2* transcripts are generally lower, seem to be uniformly distributed throughout the different tissues in the root tip, and are the highest in elongated cortical cells.

We further note that CYCD2;1-GFP stimulates LR density even in the *krp2-1* mutant background in which CYCD2;1-GFP fluorescence is not observed in the nucleus, suggesting that the targets of CYCD2;1-CDK phosphorylation may not have specific localization and that CYCD2;1 can stimulate LR density inde-

pendent of its nuclear localization. CYCD2;1 associates with CDKA (Boniotti and Gutierrez, 2001; Healy et al., 2001; Ren et al., 2008), and CYCD2;1 binds and, in complex with CDKA, phosphorylates the predominantly nuclear RBR protein (Huntley et al., 1998). Alternatives could also be envisaged, for example, that CYCD2;1 normally becomes cytoplasmic after ICK2/KRP2 destruction and that the cytoplasm is indeed its normal location of action or that cytoplasmic CYCD2;1 titrates other inhibitory proteins in the *ick2/krp2* mutant background. However, determining these possibilities will require further analysis.

A clear role for ICK/KRP proteins was found as negative regulators of CYCD2;1 action. Previously it has been found that high levels of CYCD overcome the inhibition of cell proliferation conferred by ectopic expression of *ICK/KRP* factors (Jasinski et al., 2002), and enhanced levels of ICK1/KRP1 were shown to suppress LR initiation and outgrowth (Ren et al., 2008), leading us to assay KRP proteins for their interaction with CYCD2;1. We observed that CYCD2;1 interacts strongly with ICK2/KRP2, ICK7/KRP4, and ICK5/KRP7 in a yeast-based assay, supporting earlier results (Zhou et al., 2002; Boruc et al., 2010; Van Leene et al., 2010). Through examination of loss-of-function mutants, we found that *ICK2/KRP2* suppresses LR formation, and this phenotype was further confirmed through *ICK2/KRP2* overexpression.

ICK2/KRP2 transcripts have been shown to be rapidly downregulated upon auxin-mediated pericycle reactivation (Himanen et al., 2002). We further show that auxin treatment reduces the ICK2/KRP2 protein levels and action in ICK2/KRP2-overexpressing lines. We propose that besides downregulating *ICK2/KRP2* transcription, auxin also regulates ICK2/KRP2 levels posttranscriptionally ICK1/KRP1 and ICK2/KRP2 are turned over by the 26S proteasome (Verkest et al., 2005b; Jakoby et al., 2006; Ren et al., 2008), and we speculate that a similar mechanisms is involved in downregulation of ICK2/KRP2 levels upon auxin treatment. Hence, upon auxin stimulation, *ICK2/KRP2* transcripts are downregulated, and the remaining ICK2/KRP2 protein is destroyed, resulting in an increased potential for cell division.

Recent observations implicate *ICK2/KRP2*, in concert with other inhibitors, in growth repression by DELLA proteins, since *ICK2/KRP2* is positively regulated by DELLAs (Achard et al., 2009). Together with the regulation of *ICK2/KRP2* transcripts and protein stability by auxin, the stimulation of LR density conferred by impaired *ICK2/KRP2* and the inhibition of growth and LR formation by high ICK2/KRP2 levels, this suggests that *ICK2/KRP2* is at the confluence of hormone pathways affecting growth.

We explored the possible regulation of CYCD2;1 by ICK2/KRP2 at the cellular level. Apart from in the columella stem cell population, CYCD2;1 accumulates in the nuclei of root cells. However, in the *krp2-1* mutant background, CYCD2;1 does not accumulate in the nucleus, indicating that ICK2/KRP2 influences nuclear import and/ or CYCD2;1 retention in the nucleus. In agreement with the regulation of ICK2/KRP2 levels by auxin, the effect of *krp2-1* on the cellular distribution of CYCD2;1 can be phenocopied by local triggering of auxin responses. When we investigate the cellular distribution of CYCD2;1 in tissues characterized by an auxin response maximum, such as the columella cells in primary roots and in emerged lateral primordia (Péret et al., 2009), or in artificially created response maxima, we observe that in those tissues CYCD2;1 is less strongly nuclear.

The CYCD2/KRP2 mechanism therefore contributes to the LR density response to auxin. Unlike *CYCD4;1*, whose loss of function can be overcome by auxin (Nieuwland et al., 2009), CYCD2;1 is rate-limiting for the stimulation of LR formation in response to auxin. In the *cycd4;1* mutant, cell density of cells in the basal meristem fails to increase in response to sucrose as does the LR density (Nieuwland et al., 2009). However, although *CYCD2;1* is sucrose responsive, we found no evidence for reduced cell numbers in the basal meristems of *cycd2;1* or *krp2-1* mutants (see Supplemental Figures 4A and 4B online), nor did we see a systematic change in response to auxin treatment. This suggests that the CYCD2/KRP2 mechanism affects LR density by a different mechanism involving the auxin response directly.

In conclusion, we show that the CYCD2;1/KRP2/CDKA pathway is involved in regulating LR induction in response to auxin. Under low auxin conditions, ICK2/KRP2 suppresses LR formation. The response to auxin reduces ICK2/KRP2 levels and thereby activates CYCD2;1 activity, a rate-limiting contributory factor in determining LR density.

METHODS

Plant Material and Growth Conditions

The wild-type *Arabidopsis thaliana* ecotype Col-0 was obtained from the Nottingham Arabidopsis Stock Centre. Loss-of-function *cycd2;1* and *ick2/krp2* mutants in the Col background were recovered from the Salk collection (Alonso et al., 2003). The *cycd2;1* mutant line (SALK 049449) has a T-DNA insertion in the first intron of the *CYCD2;1* gene (see Supplemental Figure 1E online). The downregulation of full-length transcripts was confirmed by RT-PCR (Dewitte et al., 2003) using primers spanning the insertion site (see Supplemental Figure 1E online) and by protein gel blot analysis using a polyclonal antibody specific against CYCD2;1 (see Supplemental Figure 1B online); no CYCD2;1 protein could be detected in this insertion line, and the *CYCD2;1* transcript level was

down to 1.7% of wild-type levels. The *krp2-1* mutant (SALK 130744) has a T-DNA insertion in exon 1 of *ICK2/KRP2*, and *krp2-3* (SALK 110338) has a T-DNA insertion in exon 3 (see Supplemental Figure 1E online). The absence of full-length transcript was confirmed by RT-PCR (see Supplemental Figure 1E online). The loss-of-function *ick1/krp1* allele *krp1-1* (SALK_100189) has an insert in the third intron of the *KRP1* gene, and no full-length transcript was detected (see Supplemental Figure 2A online). As this potentially could result in a truncated protein that lacks the CDK binding domain, the biological function was evaluated by overexpression of the fragment upstream of the T-DNA fused to a Myc domain, and no KRP OE phenotype was conferred (see Supplemental Figure 2B online). A *KRP1* full-length cDNA was cloned into the *Sma*I site of pGEM7Z vector and was fused to the C terminus of six copies of the c-myc epitope. The start codon ATG of *KRP1* was mutated to ATA using the Quikchange site-directed mutagenesis kit (Stratagene) with primers KRP1-ATG-FW and KRP1-ATG-RV. To make KRP1-C22 (ICK1/KRP1 C-terminal 22–amino acid deletion), a stop codon TAG was created using the Quikchange site-directed mutagenesis with primers KRP1-C22-FW and KRP1-C22-RV. The *Myc-KRP1* and *Myc-KRP1-C22* inserts were cloned into the *Sma*I and *Sac*I sites of the pROK2 binary vector to make the *35S:Myc-KRP1* and *35S:Myc-KRP-C22* constructs, respectively. The constructs in the binary vectors were introduced into *Agrobacterium tumefaciens* strain GV3101. Plants were transformed by vacuum infiltration (Bechtold and Pelletier, 1998). Transgenic plants were selected on ATS medium (Lincoln et al., 1990) supplemented with kanamycin.

The *ProCYCD2;1:CYCD2;1-GFP* fusion containing 3970 bp of the promoter sequence and 1710 bp of coding sequence (except the last stop codon) of the *CYCD2;1* gene and the *ProKRP2;KRP2-GFP* fusion containing 4419 of the promoter sequence and 856 bp of the coding sequence with the stop codon omitted were constructed using Gateway cloning of the PCR-amplified promoter (for primers, see Supplemental Table 1 online) plus gene fragment in the pMDC107 target vector (Karimi et al., 2007). Standard *Agrobacterium* transformation (GV3101) and floral dipping (Clough and Bent, 1998) were used to generate transformants of *Arabidopsis* Col-0. Root meristems of 25 hygromycin-resistant lines were screened for GFP fluorescence.

axr1-3, *35S:myc-ICK1/KRP* (Ren et al., 2008), and *35S:ICK2/KRP2-GFP* (Zhou et al., 2003) were previously described. *DR5:GFP* (Sabatini et al., 1999) and *35S:H2B-YFP* (Boisnard-Lorig et al., 2001) lines were kindly provided by Ben Scheres (Utrecht University, The Netherlands). Transgenic plants were selected on kanamycin- or hygromycin-containing medium. For all analysis, plants were grown vertically under a 16-h-light/8-h-dark photoperiod at 22°C on GM root medium made up from half the concentration Murashige and Skoog salts and vitamins (Duchefa), supplemented with 7.5 g/L sucrose and 15 g/L agar. Values were analyzed with the two-tailed Student's *t* test.

To assess the effect of sucrose and light on *ProCYCD2;1:CYCD2;1-GFP* expression, seedlings were grown in the dark or in the light on the modified GM medium described above with or without 7.5 g/L sucrose. To investigate induction of *ProCYCD2;1:CYCD2;1-GFP* expression, etiolated seedlings were transferred to media without (−SUC) or with (+SUC) in dark (−L) or light (+L) conditions, and CYCD2;1-GFP was imaged after 6 and 12 h.

To assess the effects of the proteasome on CYCD2;1 levels, 5-d-old *ProCYCD2;1:CYCD2;1-GFP* seedlings were transferred on the modified GM medium with or without 100 μM MG132 (Sigma-Aldrich). Fluorescence was compared after 12 h.

DR5:GFP, ProCYCD2; CYCD2;1-GFP, and 35S:KRP2-GFP lines were grown or transferred onto media supplemented with 10 μM NAA (Sigma-Aldrich) or 10 μM NPA (Sigma-Aldrich) to establish a link between sites of maximal auxin response and the dynamics of these factors.

Quantification of CYCD2;1-GFP in the Nucleus

To integrate CYCD2;1-GFP fluorescence from the three-dimensional (3D) structure of nuclei using data obtained from 3D confocal sections within nuclei, a purpose-designed algorithm, available on request, was developed. To obtain successful detection of nuclei at low contrast, a Sliding Band convergence filter was applied (Marcuzzo et al., 2009). This filter is based on gradient convergence and not on intensity, making it robust to contrast variations. This filter evaluates a convergence index for each image location, which is a function of the direction of the image gradient, and the locations of the filter response maxima correspond to cell nuclei centers. The derived information allows the full determination of the nuclear shape. Upon user intervention to identify the nuclei in a single two-dimensional section to analyze, the system searches adjacent planes for similar detections (similar in position, size, and fluorescence) and assembles a 3D array based on two-dimensional nuclei detection. Using this 3D array location and shape information, the total volume is calculated and the nuclear fluorescence is integrated. Additionally, using the nuclei's two-dimensional center's coordinates, we estimate the center line of the selected cell file and extract the cell length through edge detection.

Estimation of Protein Levels by Immunoblots

A total of 30 to 50 mg of root tissue was ground in liquid nitrogen and resuspended in 1 mL of 50 mM Tris-HCl, pH 7.5, supplemented with 75 mM NaCl, 15 mM MgCl$_2$, 1 mM DTT, 0.1% Tween 20, 1× complete Tm protease inhibitors (Roche), 1 mM NaF, 0.2 mM NaV, 2 mM Na-pyrophosphate, and 60 mM β-glycerophosphate and was homogenized four times for 30 s with 30 s on ice between homogenizations. Protein from the supernatant (15 to 20 μg) was separated on a 10% SDS-PAGE gel and transferred to a Hybond C-Super membrane (Amersham). The membrane was blocked (5% nonfat milk in PBS and 0.02% Tween 20 [PBST]) for 1 h at room temperature and incubated with a 1/1000 dilution of antiserum in 1% nonfat milk PBST overnight at room temperature. Washed membranes were incubated with peroxidase-labeled protein A (Sigma-Aldrich) in 1% nonfat milk PBST for 1 h, washed, and developed using Amersham ECL reagents. Polyclonal rabbit antibody was raised against full-length *Arabidopsis* CYCD2;1 and CDKA (Healy et al., 2001), and for the detection of the ICK2/KRP2-GFP and CYCD2;1-GFP fusion proteins, anti-GFP antiserum (ab290; Abcam) was used. Loading ratios were estimated using quantification with Image J (W.S. Rasband, U.S. National Institutes of Health; http://rsb.info.nih.gov/ij/). Myc-tagged proteins were detected as described by Ren et al. (2008).

Coimmunoprecipitation of CDKA and CYCD2;1

For immunoprecipitation, 50 μL Protein A Sepharose was added to 1 mL cell lysate, gently mixed for 1 h at 4°C, and centrifuged at 12,000*g* for 20 s (preclearing step). Five microliters of anti-CYCD2;1 antibody was added to 500 μL of the precleared solution and was incubated for 1 h at 4°C. As a negative control, nonimmune serum for the specific antibody was used. To collect immune complexes, 50 μL Protein A Sepharose 4 Fast Flow (GE Healthcare) was added and incubated for 1 h at 4°C. Immune complexes were washed three times with 1 mL of extraction buffer.

Finally, agarose beads were resuspended in 30 μL sample buffer. Protein gel blot analysis was performed as described above. The anti-CDKA;1 antibody was used at a 1:5000 dilution. The anti-CDKB1;1 and anti-CYCD2;1 antibodies (Healy et al., 2001) were used at a 1:1000 dilution of serum. The horseradish peroxidase–conjugated goat-anti-rabbit secondary antibody (Sigma-Aldrich) was used at a 1:5000 dilution.

Transcript Quantification

For quantification of transcripts, plants were grown vertically and roots were harvested upon removal of hypocotyls and shoot with a razor blade.

RNA was isolated with the TriPure isolation reagent (Roche Diagnostics), and cDNA was synthesized using the Ambion Retroscript kit. Relative quantification using real-time PCR was performed using *ACTIN* for normalization (Dewitte et al., 2003). Primer sequences for quantification of *CYCD2;1*, *CDKA;1*, and *CYCB1;1* transcripts and the analysis of insertional mutants are listed in Supplemental Table 1 online.

Yeast Two-Hybrid Assays

Yeast two-hybrid assays were performed in the yeast strain MaV203. *ICK/KPR* cDNA constructs (Zhou et al., 2002) of *ICK/KRP* genes to be tested for interactions were cloned using *Sal*I and *Not*I sites in pPC86 (Chevray and Nathans, 1992) (for *ICK1/KRP1*, *ICK2/KRP2*, *ICK6/KRP3*, *ICK7/KRP4*, and *ICK3/KRP5*) or pBI771 (Kohalmi et al., 1997) (for *ICK4/KRP6* and *ICK5/KRP7*). Truncated (TR) and full-length (FL) cDNAs of the native *CYCD2;1* gene were obtained as described previously (Qi and John, 2007), and they were cloned in pBI880 (BD vector) using *Sal*I and *Not*I sites, a derivative of pPC62 (Chevray and Nathans, 1992). The *CYCD2;1* nonspliceable variant gene was generated using PCR amplification with overlapping primers (sets 1 and 2; see Supplemental Table 1 online) that contained specific changes to remove splice sites without changing the encoded amino acids. Transformation of the yeast strain MaV203 was performed and grown on selective SD medium prepared according to the manufacturer's instructions (Life Technologies). Colonies growing on selective medium were assayed for *LACZ* encoded β-galactosidase activity (Duttweiler, 1996). *CDKA;1* and *CDKB;1 AD* and *BD* fusions were created by Gateway cloning (Invitrogen) by LR reaction using Gateway vectors pDEST22 (AD vector; Invitrogen) and pDEST32 (BD vector; Invitrogen) and pENTR-TOPO (Invitrogen) CDKA;1 and CDKB1;1 clones, generated according to the manufacturer's instructions with the primers listed in Supplemental Table 1 online.

For yeast three-hybrid assays, the yeast strain PJ69-4A (James et al., 1996) was cotransformed with three different plasmids: vectors (described above) containing the GAL4 DNA BD fused to *CYCD2;1-FL*, *CDKA;1*, or *CDKB1;1*, vectors containing the AD fused to *ICK2/KRP2*, *CDKA;1*, or *CDKB1;1* (described above), and either the empty vectors pPC86 and pFL61 (Minet et al., 1992) or pFL61 expressing the *ICK2/KRP2* gene, obtained upon cutting *ICK2/KRP2* out of pPC86 with *Sal*I and *Not*I and introducing it into the *Not*I site after blunting, under a constitutive *PGK* promoter. The transformants were selected on SD medium lacking Trp, Leu, and uracil. Colonies were grown overnight at 30°C in liquid SD medium supplemented with the required amino acids, and 10 μL of the suspension was spotted onto SD selective agar plates. Interaction between BD and AD fusion proteins was scored by the relative yeast growth on SD media lacking His (−His) and containing 30 mM 3-amino-1,2,4 triazole or lacking adenine (−Ade) and by β-galactosidase assay.

Confocal Microscopy

Pericycle cell sizes in RAMs were measured as described (Nieuwland et al., 2009). For live imaging of GFP and YFP, cell walls in roots were counterstained with 4 μg/mL propidium iodide in water, and GFP, YFP, and PI fluorescence was examined with a Zeiss 510 Meta or Zeiss 710 Meta confocal microscope.

Accession Numbers

Sequence data from this article can be found in the Arabidopsis Genome Initiative or GenBank/EMBL databases under the following accession numbers: *CYCD2;1*, At2g22490; *ICK1/KRP1*, At2g23430; *ICK2/KRP2*, At3g50630; *ICK6/KRP3*, At5g48820; *ICK7KRP4*, At2g32710; *ICK3/KRP5*, At3g24810; *ICK4/KRP6*, At3g19150; *ICK5/KRP7* At1g49620; *CDKA;1*, At3g48750; *CDKB1;1*, At3g54180; and *CYCB1;1*, At4g37490.

Supplemental Data

The following materials are available in the online version of this article.

  Supplemental Figure 1. Additional Functional Aspects of CYCD2;1 and Characterization of *cycd2;1* and *ick2/krp2* Mutant Alleles.

  Supplemental Figure 2. Characterization of *ick1/krp1* Mutant Alleles.

  Supplemental Figure 3. Loading Controls for Figures 6B and 6C.

  Supplemental Figure 4. Pericycle Cell Length in the Basal Meristem of *ick2/krp2* and *cycd2;1* Mutants Is Not Systematically Altered.

  Supplemental Table 1. Primer Sequences Used.

REFERENCES

Achard, P., Gusti, A., Cheminant, S., Alioua, M., Dhondt, S., Coppens, F., Beemster, G.T., and Genschik, P. (2009). Gibberellin signaling controls cell proliferation rate in *Arabidopsis.* Curr. Biol. **19:** 1188–1193.

Alonso, J.M., et al. (2003). Genome-wide insertional mutagenesis of *Arabidopsis thaliana.* Science **301:** 653–657.

Baluska, F., Mancuso, S., Volkmann, D., and Barlow, P.W. (2010). Root apex transition zone: A signalling-response nexus in the root. Trends Plant Sci. **15:** 402–408.

Bechtold, N., and Pelletier, G. (1998). In planta *Agrobacterium*-mediated transformation of adult *Arabidopsis thaliana* plants by vacuum infiltration. Methods Mol. Biol. **82:** 259–266.

Bird, D.A., Buruiana, M.M., Zhou, Y., Fowke, L.C., and Wang, H. (2007). *Arabidopsis* cyclin-dependent kinase inhibitors are nuclear-localized and show different localization patterns within the nucleoplasm. Plant Cell Rep. **26:** 861–872.

Boerjan, W., Cervera, M.T., Delarue, M., Beeckman, T., Dewitte, W., Bellini, C., Caboche, M., Van Onckelen, H., Van Montagu, M., and Inzé, D. (1995). Superroot, a recessive mutation in *Arabidopsis*, confers auxin overproduction. Plant Cell **7:** 1405–1419.

Boisnard-Lorig, C., Colon-Carmona, A., Bauch, M., Hodge, S., Doerner, P., Bancharel, E., Dumas, C., Haseloff, J., and Berger, F. (2001). Dynamic analyses of the expression of the HISTONE:YFP fusion protein in *Arabidopsis* show that syncytial endosperm is divided in mitotic domains. Plant Cell **13:** 495–509.

Boniotti, M.B., and Gutierrez, C. (2001). A cell-cycle-regulated kinase activity phosphorylates plant retinoblastoma protein and contains, in *Arabidopsis*, a CDKA/cyclin D complex. Plant J. **28:** 341–350.

Boruc, J., Van den Daele, H., Hollunder, J., Rombauts, S., Mylle, E., Hilson, P., Inzé, D., De Veylder, L., and Russinova, E. (2010). Functional modules in the *Arabidopsis* core cell cycle binary protein-protein interaction network. Plant Cell **22:** 1264–1280.

Brady, S.M., Orlando, D.A., Lee, J.Y., Wang, J.Y., Koch, J., Dinneny, J.R., Mace, D., Ohler, U., and Benfey, P.N. (2007). A high-resolution root spatiotemporal map reveals dominant expression patterns. Science **318:** 801–806.

Casimiro, I., Beeckman, T., Graham, N., Bhalerao, R., Zhang, H., Casero, P., Sandberg, G., and Bennett, M.J. (2003). Dissecting *Arabidopsis* lateral root development. Trends Plant Sci. **8:** 165–171.

Casimiro, I., Marchant, A., Bhalerao, R.P., Beeckman, T., Dhooge, S., Swarup, R., Graham, N., Inzé, D., Sandberg, G., Casero, P.J., and Bennett, M. (2001). Auxin transport promotes *Arabidopsis* lateral root initiation. Plant Cell **13:** 843–852.

Chevray, P.M., and Nathans, D. (1992). Protein interaction cloning in yeast: Identification of mammalian proteins that react with the leucine zipper of Jun. Proc. Natl. Acad. Sci. USA **89:** 5789–5793.

Churchman, M.L., et al. (2006). SIAMESE, a plant-specific cell cycle regulator, controls endoreplication onset in *Arabidopsis thaliana*. Plant Cell **18:** 3145–3157.

Cleary, A., Fowke, L., Wang, H., and John, P. (2002). The effect of ICK1, a plant cyclin-dependent kinase inhibitor, on mitosis in living plant cells. Plant Cell Rep. **20:** 814–820.

Clough, S.J., and Bent, A.F. (1998). Floral dip: a simplified method for Agrobacterium-mediated transformation of *Arabidopsis thaliana.* Plant J. **16:** 735–743.

Cockcroft, C.E., den Boer, B.G., Healy, J.M., and Murray, J.A.H. (2000). Cyclin D control of growth rate in plants. Nature **405:** 575–579.

De Smet, I., Vanneste, S., Inzé, D., and Beeckman, T. (2006). Lateral root initiation or the birth of a new meristem. Plant Mol. Biol. **60:** 871–887.

De Smet, I., et al. (2007). Auxin-dependent regulation of lateral root positioning in the basal meristem of *Arabidopsis.* Development **134:** 681–690.

De Smet, I., et al. (2010). Bimodular auxin response controls organogenesis. Proc. Natl. Acad. Sci. USA **107:** 2705–2710.

De Veylder, L., Beeckman, T., Beemster, G.T., de Almeida Engler, J., Ormenese, S., Maes, S., Naudts, M., Van Der Schueren, E., Jacqmard, A., Engler, G., and Inzé, D. (2002). Control of proliferation, endoreduplication and differentiation by the *Arabidopsis* E2Fa-DPa transcription factor. EMBO J. **21:** 1360–1368.

De Veylder, L., Beeckman, T., Beemster, G.T., Krols, L., Terras, F., Landrieu, I., van der Schueren, E., Maes, S., Naudts, M., and Inzé, D. (2001). Functional analysis of cyclin-dependent kinase inhibitors of *Arabidopsis.* Plant Cell **13:** 1653–1668.

De Veylder, L., de Almeida Engler, J., Burssens, S., Manevski, A., Lescure, B., Van Montagu, M., Engler, G., and Inzé, D. (1999). A new D-type cyclin of *Arabidopsis thaliana* expressed during lateral root primordia formation. Planta **208:** 453–462.

Dewitte, W., and Murray, J.A.H. (2003). The plant cell cycle. Annu. Rev. Plant Biol. **54:** 235–264.

Dewitte, W., Riou-Khamlichi, C., Scofield, S., Healy, J.M., Jacqmard, A., Kilby, N.J., and Murray, J.A.H. (2003). Altered cell cycle distribution, hyperplasia, and inhibited differentiation in *Arabidopsis* caused by the D-type cyclin CYCD3. Plant Cell **15:** 79–92.

Dewitte, W., Scofield, S., Alcasabas, A.A., Maughan, S.C., Menges, M., Braun, N., Collins, C., Nieuwland, J., Prinsen, E., Sundaresan, V., and Murray, J.A.H. (2007). *Arabidopsis* CYCD3 D-type cyclins link cell proliferation and endocycles and are rate-limiting for cytokinin responses. Proc. Natl. Acad. Sci. USA **104:** 14537–14542.

Dharmasiri, N., Dharmasiri, S., Weijers, D., Karunarathna, N., Jurgens, G., and Estelle, M. (2007). AXL and AXR1 have redundant functions in RUB conjugation and growth and development in Arabidopsis. Plant J. **52:** 114–123.

Ditengou, F.A., Teale, W.D., Kochersperger, P., Flittner, K.A., Kneuper, I., van der Graaff, E., Nziengui, H., Pinosa, F., Li, X., Nitschke, R., Laux, T., and Palme, K. (2008). Mechanical induction of lateral root initiation in *Arabidopsis thaliana.* Proc. Natl. Acad. Sci. USA **105:** 18818–18823.

Dubrovsky, J.G., Rost, T.L., Colón-Carmona, A., and Doerner, P. (2001). Early primordium morphogenesis during lateral root initiation in *Arabidopsis thaliana.* Planta **214:** 30–36.

Dubrovsky, J.G., Sauer, M., Napsucialy-Mendivil, S., Ivanchenko, M. G., Friml, J., Shishkova, S., Celenza, J., and Benková, E. (2008). Auxin acts as a local morphogenetic trigger to specify lateral root founder cells. Proc. Natl. Acad. Sci. USA **105:** 8790–8794.

Duttweiler, H.M. (1996). A highly sensitive and non-lethal beta-galactosidase plate assay for yeast. Trends Genet. **12:** 340–341.

Ebel, C., Mariconti, L., and Gruissem, W. (2004). Plant retinoblastoma homologues control nuclear proliferation in the female gametophyte. Nature **429:** 776–780.

Fukaki, H., Tameda, S., Masuda, H., and Tasaka, M. (2002). Lateral root formation is blocked by a gain-of-function mutation in the SOLITARY-ROOT/IAA14 gene of *Arabidopsis.* Plant J. **29:** 153–168.

Fukaki, H., and Tasaka, M. (2009). Hormone interactions during lateral root formation. Plant Mol. Biol. **69:** 437–449.

Healy, J.M., Menges, M., Doonan, J.H., and Murray, J.A.H. (2001). The *Arabidopsis* D-type cyclins CycD2 and CycD3 both interact in vivo with the PSTAIRE cyclin-dependent kinase Cdc2a but are differentially controlled. J. Biol. Chem. **276:** 7041–7047.

Himanen, K., Boucheron, E., Vanneste, S., de Almeida Engler, J., Inzé, D., and Beeckman, T. (2002). Auxin-mediated cell cycle activation during early lateral root initiation. Plant Cell **14:** 2339–2351.

Himanen, K., Vuylsteke, M., Vanneste, S., Vercruysse, S., Boucheron, E., Alard, P., Chriqui, D., Van Montagu, M., Inzé, D., and Beeckman, T. (2004). Transcript profiling of early lateral root initiation. Proc. Natl. Acad. Sci. USA **101:** 5146–5151.

Hirano, H., Harashima, H., Shinmyo, A., and Sekine, M. (2008). *Arabidopsis* RETINOBLASTOMA-RELATED PROTEIN 1 is involved in G1 phase cell cycle arrest caused by sucrose starvation. Plant Mol. Biol. **66:** 259–275.

Huntley, R., et al. (1998). The maize retinoblastoma protein homologue ZmRb-1 is regulated during leaf development and displays conserved interactions with G1/S regulators and plant cyclin D (CycD) proteins. Plant Mol. Biol. **37:** 155–169.

Inzé, D., and De Veylder, L. (2006). Cell cycle regulation in plant development. Annu. Rev. Genet. **40:** 77–105.

Jakoby, M.J., Weinl, C., Pusch, S., Kuijt, S.J., Merkle, T., Dissmeyer, N., and Schnittger, A. (2006). Analysis of the subcellular localization, function, and proteolytic control of the *Arabidopsis* cyclin-dependent kinase inhibitor ICK1/KRP1. Plant Physiol. **141:** 1293–1305.

James, P., Halladay, J., and Craig, E.A. (1996). Genomic libraries and a host strain designed for highly efficient two-hybrid selection in yeast. Genetics **144:** 1425–1436.

Jasinski, S., Riou-Khamlichi, C., Roche, O., Perennes, C., Bergounioux, C., and Glab, N. (2002). The CDK inhibitor NtKIS1a is involved in plant development, endoreduplication and restores normal development of cyclin D3;1-overexpressing plants. J. Cell Sci. **115:** 973–982.

Karimi, M., Depicker, A., and Hilson, P. (2007). Recombinational cloning with plant gateway vectors. Plant Physiol. **145:** 1144–1154.

Kohalmi, S.E., Nowak, J., and Crosby, W. L. (1997). The yeast two-hybrid system. In Differentially Expressed Genes in Plants: A Bench

Manual, E. Hansen and G. Harper, eds (London: Taylor & Francis), pp. 63–82.

Laskowski, M., Grieneisen, V.A., Hofhuis, H., Hove, C.A., Hogeweg, P., Marée, A.F., and Scheres, B. (2008). Root system architecture from coupling cell shape to auxin transport. PLoS Biol. **6:** e307.

Laskowski, M.J., Williams, M.E., Nusbaum, H.C., and Sussex, I.M. (1995). Formation of lateral root meristems is a two-stage process. Development **121:** 3303–3310.

Lechner, E., Xie, D., Grava, S., Pigaglio, E., Planchais, S., Murray, J.A.H., Parmentier, Y., Mutterer, J., Dubreucq, B., Shen, W.H., and Genschik, P. (2002). The AtRbx1 protein is part of plant SCF complexes, and its down-regulation causes severe growth and developmental defects. J. Biol. Chem. **277:** 50069–50080.

Lincoln, C., Britton, J.H., and Estelle, M. (1990). Growth and development of the *axr1* mutants of *Arabidopsis.* Plant Cell **2:** 1071–1080.

López-Bucio, J., Cruz-Ramírez, A., and Herrera-Estrella, L. (2003). The role of nutrient availability in regulating root architecture. Curr. Opin. Plant Biol. **6:** 280–287.

Marcuzzo, M., Quelhas, P., Campilho, A., Mendonça, A.M., and Campilho, A. (2009). Automated *Arabidopsis* plant root cell segmentation based on SVM classification and region merging. Comput. Biol. Med. **39:** 785–793.

Masubelele, N.H., Dewitte, W., Menges, M., Maughan, S., Collins, C., Huntley, R., Nieuwland, J., Scofield, S., and Murray, J.A.H. (2005). D-type cyclins activate division in the root apex to promote seed germination in *Arabidopsis.* Proc. Natl. Acad. Sci. USA **102:** 15694–15699.

Menges, M., de Jager, S.M., Gruissem, W., and Murray, J.A.H. (2005). Global analysis of the core cell cycle regulators of *Arabidopsis* identifies novel genes, reveals multiple and highly specific profiles of expression and provides a coherent model for plant cell cycle control. Plant J. **41:** 546–566.

Menges, M., Samland, A.K., Planchais, S., and Murray, J.A.H. (2006). The D-type cyclin CYCD3;1 is limiting for the G1-to-S-phase transition in *Arabidopsis.* Plant Cell **18:** 893–906.

Minet, M., Dufour, M.E., and Lacroute, F.B. (1992). Complementation of *Saccharomyces cerevisiae* auxotrophic mutants by *Arabidopsis thaliana* cDNAs. Plant J. **2:** 417–422.

Moreno-Risueno, M.A., Van Norman, J.M., Moreno, A., Zhang, J., Ahnert, S.E., and Benfey, P.N. (2010). Oscillating gene expression determines competence for periodic *Arabidopsis* root branching. Science **329:** 1306–1311.

Nieuwland, J., Maughan, S., Dewitte, W., Scofield, S., Sanz, L., and Murray, J.A.H. (2009). The D-type cyclin CYCD4;1 modulates lateral root density in *Arabidopsis* by affecting the basal meristem region. Proc. Natl. Acad. Sci. USA **106:** 22528–22533.

Okushima, Y., Fukaki, H., Onoda, M., Theologis, A., and Tasaka, M. (2007). ARF7 and ARF19 regulate lateral root formation via direct activation of LBD/ASL genes in *Arabidopsis.* Plant Cell **19:** 118–130.

Péret, B., De Rybel, B., Casimiro, I., Benková, E., Swarup, R., Laplaze, L., Beeckman, T., and Bennett, M.J. (2009). *Arabidopsis* lateral root development: An emerging story. Trends Plant Sci. **14:** 399–408.

Petersson, S.V., Johansson, A.I., Kowalczyk, M., Makoveychuk, A., Wang, J.Y., Moritz, T., Grebe, M., Benfey, P.N., Sandberg, G., and Ljung, K. (2009). An auxin gradient and maximum in the *Arabidopsis* root apex shown by high-resolution cell-specific analysis of IAA distribution and synthesis. Plant Cell **21:** 1659–1668.

Petroski, M.D., and Deshaies, R.J. (2005). Function and regulation of cullin-RING ubiquitin ligases. Nat. Rev. Mol. Cell Biol. **6:** 9–20.

Planchais, S., Samland, A.K., and Murray, J.A.H. (2004). Differential stability of *Arabidopsis* D-type cyclins: CYCD3;1 is a highly unstable

protein degraded by a proteasome-dependent mechanism. Plant J. **38:** 616–625.

Qi, R., and John, P.C. (2007). Expression of genomic AtCYCD2;1 in *Arabidopsis* induces cell division at smaller cell sizes: Implications for the control of plant growth. Plant Physiol. **144:** 1587–1597.

Ren, H., Santner, A., del Pozo, J.C., Murray, J.A.H., and Estelle, M. (2008). Degradation of the cyclin-dependent kinase inhibitor KRP1 is regulated by two different ubiquitin E3 ligases. Plant J. **53:** 705–716.

Richter, G.L., Monshausen, G.B., Krol, A., and Gilroy, S. (2009). Mechanical stimuli modulate lateral root organogenesis. Plant Physiol. **151:** 1855–1866.

Riou-Khamlichi, C., Huntley, R., Jacqmard, A., and Murray, J.A.H. (1999). Cytokinin activation of Arabidopsis cell division through a D-type cyclin. Science **283:** 1541–1544.

Riou-Khamlichi, C., Menges, M., Healy, J.M., and Murray, J.A.H. (2000). Sugar control of the plant cell cycle: differential regulation of Arabidopsis D-type cyclin gene expression. Mol. Cell. Biol. **20:** 4513–4521.

Sabatini, S., Beis, D., Wolkenfelt, H., Murfett, J., Guilfoyle, T., Malamy, J., Benfey, P., Leyser, O., Bechtold, N., Weisbeek, P., and Scheres, B. (1999). An auxin-dependent distal organizer of pattern and polarity in the Arabidopsis root. Cell **99:** 463–472.

Schnittger, A., Schöbinger, U., Bouyer, D., Weinl, C., Stierhof, Y.D., and Hülskamp, M. (2002). Ectopic D-type cyclin expression induces not only DNA replication but also cell division in *Arabidopsis* trichomes. Proc. Natl. Acad. Sci. USA **99:** 6410–6415.

Van Leene, J., et al. (2010). Targeted interactomics reveals a complex core cell cycle machinery in *Arabidopsis thaliana.* Mol. Syst. Biol. **6:** 397.

Vanneste, S., et al. (2005). Cell cycle progression in the pericycle is not sufficient for SOLITARY ROOT/IAA14-mediated lateral root initiation in *Arabidopsis thaliana.* Plant Cell **17:** 3035–3050.

Verkest, A., Manes, C.L., Vercruysse, S., Maes, S., Van Der Schueren, E., Beeckman, T., Genschik, P., Kuiper, M., Inzé, D., and De Veylder, L. (2005b). The cyclin-dependent kinase inhibitor KRP2 controls the onset of the endoreduplication cycle during *Arabidopsis* leaf development through inhibition of mitotic CDKA;1 kinase complexes. Plant Cell **17:** 1723–1736.

Verkest, A., Weinl, C., Inzé, D., De Veylder, L., and Schnittger, A. (2005a). Switching the cell cycle. Kip-related proteins in plant cell cycle control. Plant Physiol. **139:** 1099–1106.

Wang, H., Qi, Q., Schorr, P., Cutler, A.J., Crosby, W.L., and Fowke, L.C. (1998). ICK1, a cyclin-dependent protein kinase inhibitor from *Arabidopsis thaliana* interacts with both Cdc2a and CycD3, and its expression is induced by abscisic acid. Plant J. **15:** 501–510.

Wildwater, M., Campilho, A., Perez-Perez, J.M., Heidstra, R., Blilou, I., Korthout, H., Chatterjee, J., Mariconti, L., Gruissem, W., and Scheres, B. (2005). The RETINOBLASTOMA-RELATED gene regulates stem cell maintenance in *Arabidopsis* roots. Cell **123:** 1337–1349.

Willemse, J., Kulikova, O., de Jong, H., and Bisseling, T. (2008). A new whole-mount DNA quantification method and the analysis of nuclear DNA content in the stem-cell niche of *Arabidopsis* roots. Plant J. **55:** 886–894.

Winter, D., Vinegar, B., Nahal, H., Ammar, R., Wilson, G.V., and Provart, N.J. (2007). An "Electronic Fluorescent Pictograph" browser for exploring and analyzing large-scale biological data sets. PLoS ONE **2:** e718.

Zhou, Y., Fowke, L.C., and Wang, H. (2002). Plant CDK inhibitors: Studies of interactions with cell cycle regulators in the yeast two-hybrid system and functional comparisons in transgenic *Arabidopsis* plants. Plant Cell Rep. **20:** 967–975.

Zhou, Y., Niu, H., Brandizzi, F., Fowke, L.C., and Wang, H. (2006). Molecular control of nuclear and subnuclear targeting of the plant CDK inhibitor ICK1 and ICK1-mediated nuclear transport of CDKA. Plant Mol. Biol. **62:** 261–278.

Zhou, Y., Wang, H., Gilmer, S., Whitwill, S., and Fowke, L.C. (2003). Effects of co-expressing the plant CDK inhibitor ICK1 and D-type cyclin genes on plant growth, cell size and ploidy in *Arabidopsis thaliana.* Planta **216:** 604–613.